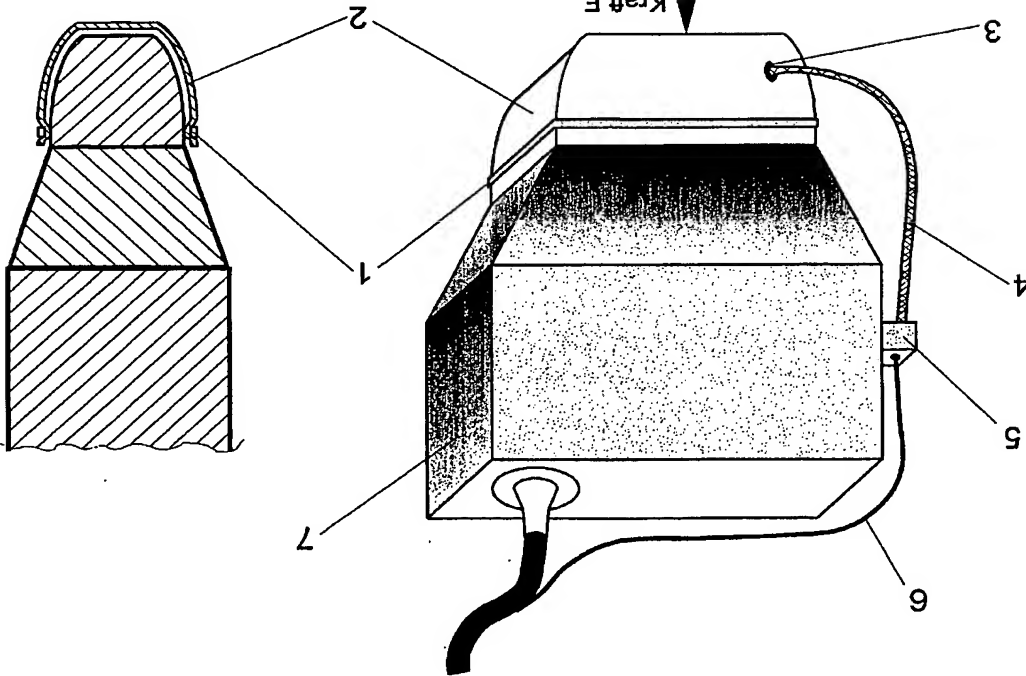


Nummer:
DE 197 54 085 A1
G 01 N 29/04
Offenlegungstag:
10. Juni 1999



Skizze 4: Nichtendoskopische Ultraschallsonde

902 023/471

DE 197 54 085 A 1



Offenlegungsschrift **DE 197 54 085 A 1**

① BUNDESREPUBLIK
DEUTSCHLAND



DEUTSCHES
PATENT- UND
MARKENAMT

② Int. Cl.⁶
G 01 N 29/04
G 01 N 33/12

③ Aktenzeichen: 197 54 085.6
④ Anmeldetag: 5. 12. 97
⑤ Offenlegungstag: 10. 6. 99

DE 197 54 085 A 1

⑦ Anmelder:

Ermert, Helmut, Prof. Dr.-Ing., 91341 Röttenbach,
DE; Lorenz, Andreas, Dipl.-Ing., 44789 Bochum, DE;
Wiebe, Peter, Dipl.-Ing., 58235 Gelvesberg, DE

⑦ Erfinder:

gleich Anmelder

Die folgenden Angaben sind den vom Anmelder eingereichten Unterlagen entnommen
⑧ Ein sonographisches Elastographiesystem

Beschreibung

Die Erfindung betrifft eine Meßeinrichtung entsprechend dem Oberbegriff des Anspruchs 1.

Anwendungsgebiet

Die mechanischen Eigenschaften von biologischen Gewebe (z. B. Elastizitätsparameter) sind für die Beurteilung des Zustandes des Gewebes von großem Interesse. In der medizinischen Diagnostik dienen Verformungen der elastischen Eigenschaften auf histologische und u. U. pathologische Veränderungen hin. Allgemein bekannt sind Prozeduren wie die Bildung von Geschwulsten und Verhärtungen ("Knoten"), die z. B. manuell tastbar sind. In der Landwirtschaft ist für die Beurteilung der Qualität des Fleisches von Schlachttvieh die Kenntnis mechanischer Gewbeeigenschaften ebenfalls von Interesse.

Stand der Technik

Die sogenannte Tastbefundung ist ungenau und unempfindlich. Wesentlich besser ist in dieser Beziehung die sogenannte Elastographie, bei der elastische Gewbeeigenschaften technisch erfasst und z. B. in Form von Schallbildern qualitativ oder quantitativ visualisiert werden. Dabei bedient man sich hauptsächlich des Ultraschalls, wie er als bildgebendes Verfahren in der medizinischen Diagnostik angewandt wird. In zeitlich nacheinander aufgenommenen Ultraschallbildern können geringe Verschiebungen oder Verformungen innerhalb der Ultraschall-Gewebestruktur durch Auswertung der Bildsequenzen erfasst und ausgewertet werden. Wird auf einen Gewebebereich ein mechanischer Druck ausgeübt, der eine Verformung des Gewebes zur Folge hat, so verändern sich Bereiche mit unterschiedlichen Elastizitätseigenschaften verschiebenartig. Das Elastographie-System weist diese Verformungen durch den numerischen Vergleich der Einzelbilder aus und stellt die unterschiedlichen Elastizitätsgrenzen im Bild dar. Die notwendige Kompression des Gewebes, die z. B. extern provoziert wird, ist nur gering und bedingt bei Anwendung des üblichen diagnostischen Ultraschalls nur Bruchteile von Millimetern. Wichtig dabei ist eine quantitative Kontrolle des Kompressionsdrucks.

Ein Verfahren der Ultraschall-Elastographie von Körpergewebe ist erstmals in einem Aufsatz von J. Ophir et al. im Jahre 1991 [1], [2] beschrieben worden. Dabei werden Ultraschallbilder bzw. die korrespondierenden hochfrequenten Ultraschallsignale so ausgewertet, daß Verschiebungen des Körpergewebes zwischen zwei, mit verschiedener Kompression aufgenommenen Gewebeschichten berechnet werden. Auf diese Weise lassen sich die bereits erhaltene Rückmeldung auf die Elastizität des Organs bis hin zu einer quantitativen Abbildung des Elastizitätsmoduls erzielen.

In der Literatur werden verschiedene Ansätze vorgestellt, mit denen die Abbildungseigenschaften eines Elastographie-Systems verbessert werden können. Weiterverfolgend im Hinblick auf das Signal-Rauschverhältnis und den Kontrast der Elastographiebilder sind Ansätze, die mehrfache Kompressionsstufen des abzubildenden Gewebes auswerfen [5]. Bei diesen Ansätzen werden bis zu 120 Bilder in einer Aufnahmeseite aufgenommen und mit bekannten Methoden der Ultraschall-Elastographie [3], [4] weiterverarbeitet.

Nachteile des Standes der Technik

Ein Nachteil der bisher publizierten bzw. praktizierten Verfahren ist, daß zu keiner Zeit die Kraft auf das Gewebe

bekannt ist, die wertvolle Informationen bei einer quantitativen Rekonstruktion des Flüssigkeitsmoduls liefern kann. Außerdem ist ein solcher Ansatz speicher- und rechenintensiv, da Auswertearbeiten dazu herangezogen werden müssen, optimale Bildfolgen aus den aufgenommenen Daten auszuwählen und weiterzuverarbeiten.

Aufgabe der Erfindung

Die Aufgabe der Erfindung ist es, Ultraschallbilder in vorgegebenen Kompressionsstufen aufzunehmen, um eine Anzeige der elastischen Eigenschaften von Körpergewebe einzufügen zu machen und durch genaue Messung und Kontrolle des applizierten Druckes eine quantitative Rekonstruktion des Elastizitätsmoduls zu unterstützen.

Lösung der Aufgabe

Diese Aufgabe wird durch ein Meßsystem mit den Merkmalen des Anspruchs 1 gelöst.

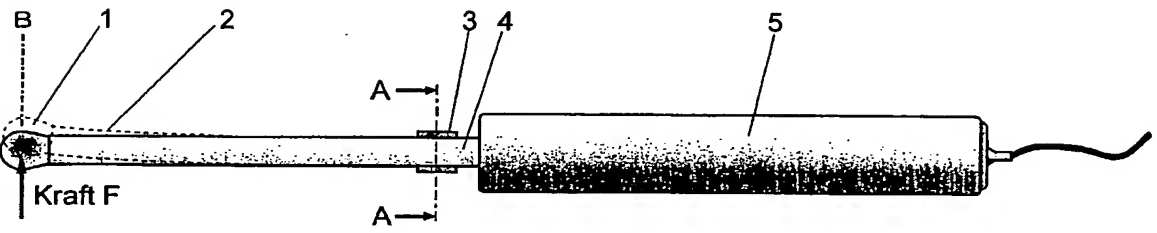
Die Kompression des Gewebes wird durch den Ultraschallwandler, mit dem die Ultraschallbilder aufgenommen werden, hervorgerufen. Die Kraft, die der Schallwandler auf das Gewebe ausübt, wird durch eine mit diesem Wandler verbundene Vorrichtung gemessen, und es werden Ultraschallbilder in vorgegebenen Kompressionsstufen aufgenommen. Insbesondere läßt sich bei endoskopischen Schallköpfen, (z. B. bei einer transrektalen oder transvaginalen Sonde), die für gezielte Kalibrierungen nur wenig Platz erlauben, die Kraft mittels eines am Schallkopf-Schallkopf angebrachten Dehnungssensors nach dem Bragg-Schallkopfprinzip bestimmen. Für nicht-endoskopische Schallköpfe, d. h. Schallköpfe, die auf der Körperoberfläche appliziert werden, kann eine wassergefüllte, schalldurchlässige Kappe auf dem Schallkopf angebracht werden. Eine Kraftmessung ist dann mittels eines hydrostatischen Drucksensors möglich.

Vorteile der Erfindung

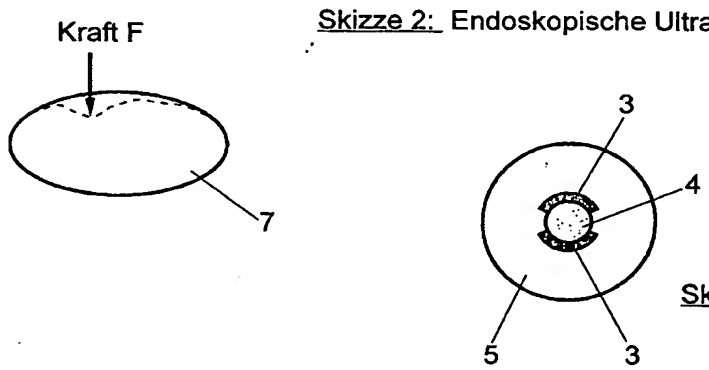
Dieser Ansatz erlaubt eine Montage der Sensoren auf handelsübliche Ultraschallsonden mit nur geringfügiger Modifikation der Schallköpfe. Es werden keine geräuschhaften Veränderungen am Ultraschallgerät vorgenommen. Kraft- bzw. Drucksensoren, was den Spektren- und Rechenaufwand im Vergleich zu bekannten Ansätzen erheblich reduziert. Die Erfindung macht bei der Anwendung starrer endoskopischer Schallköpfe eine quantitative Elastographie erst möglich.

Literaturangaben

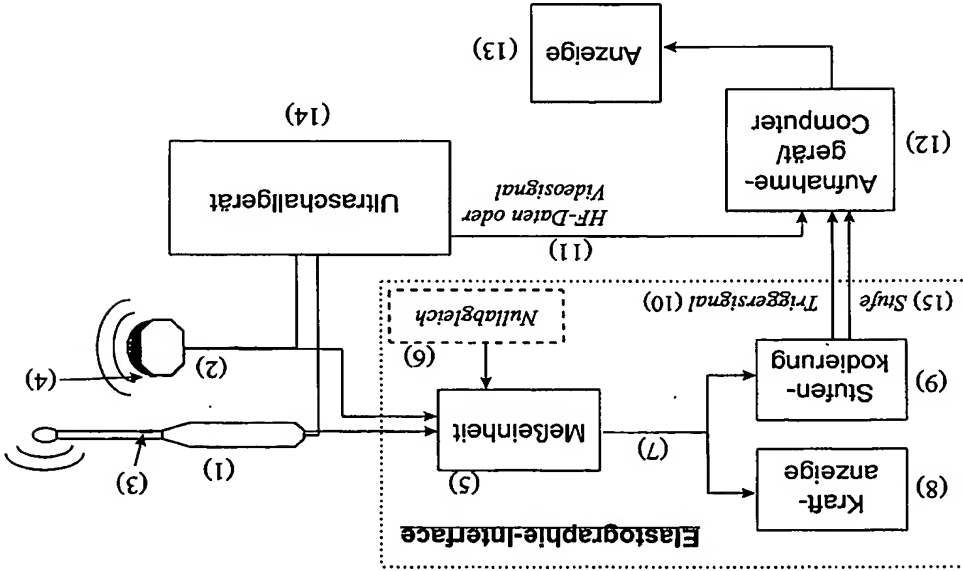
- [1] Ophir J., Céspedes I., Ponnekanti H., Yazdi Y., Li X.: Elastography: A quantitative method for imaging the elasticity of biological tissues. Ultrasonic imaging 13, 111-114, 1991.
- [2] Céspedes I., Ophir J., Ponnekanti H., Maklad N.: Elastography: Elasticity imaging using ultrasound with application to muscle and breast imaging in vivo. Ultrasonic Imaging 15, 73-88, 1993.
- [3] O'Donnell M., Skovoroda A. R., Shapo D. M., Emilianov S. Y.: Internal displacement and strain imaging using ultrasonic speckle tracking. IEEE transactions on ultrasonics ferroelectrics and frequency control, 41, 314-325, May 1994.
- [4] Lubinski M. A., Emilianov S. Y., Raghuvaran K. R.: Latent displacement estimation using tissue incompressibility.



Skizze 2: Endoskopische Ultraschallsonde (schematisch)



Skizze 3: Schnitt A-A zu Skizze 2



Skizze 1: Schematische Darstellung des Elastographie-Messsystems

IEEE transactions on ultrasonics ferroelectrics and frequency control, 43, 234-246, 1995.
 [5] Emilianov S. Y., Lobinski M. A., Skovoroda A. R., Erkamp R. Q., Leavay S. F., Wiggins R. C., O'Donnell M.: Resonant ultrasound elastography: imaging for renal pathology detection. Proc. 1997 IEEE Ultrasonics Symposium, IEEE Press, Piscataway, MD, USA.

B. Beispielschreibung einer Patentanmeldung

Ausführungszeichnungen der Erfindung sind in den Zeichnungen dargestellt und werden im folgenden näher beschrieben.

Zu Skizze 1: Schematische Darstellung des Elastographie-Messsystems

Das Messsystem besteht im wesentlichen aus drei Funktionseinheiten:

- Ein handelsübliches Ultraschallsystem mit verschiedenen endoskopischen und nicht-endoskopischen Sonden. Am Ultraschallgerät muß dabei eine Möglichkeit zur Aufnahme von Video oder HF-Daten bestehen.
- Eine Interfaceeinheit (in Skizze 1 mit Elastographie-Interface bezeichnet) die zur Anzeige des Druckes und zur Umwandlung der Sensorsignale in korrespondierende Triggersignale verwendet wird. Die Triggersignale entsprechen dabei den verschiedenen Kompressionsstufen.
- Eine Computereinheit, die mit entsprechenden Peripheriegeräten ausgerüstet ist (z. B. A/D-Wandler, Framegrabberkarte), und zur Datenaufnahme und weiterverarbeitung verwendet wird.

Kernstück der Erfindung ist die Einrichtung zur Messung der Kraft, die auf das Gewebe ausgeübt wird, und zur Erzeugung von Triggersignalen zur Bildaufnahme. Dazu sind an der endoskopischen Sonde (1) ein oder mehrere Dehnungssensoren (5) angebracht. Ein Ausführungsbeispiel zu dieser Art der Kraftmessung ist in den Skizzen 2 und 3 dargestellt. An nicht-endoskopischen Sonden (2) wird eine wassergefüllte Kappe aus schalldurchlässigem Material angebracht. Der hydrostatische Wasserdruck in der Kappe kann dann mittels eines Drucksensors (4) gemessen werden. Ein Ausführungsbeispiel einer nicht-endoskopischen Sonde ist in der Skizze 4 dargestellt.

Die Sensorsignale werden einer Messeinheit (5) zugeführt. Üblicherweise wird hier eine Brückenschaltung eingesetzt, die bei kleinen Biegungen bzw. kleinen Druckänderungen eine zur Kraft proportionale Spannung (7) liefert. Um einen definierten Anfangszustand zu erzielen, muß die Messeinheit abgeglich werden (6). Das Ausgangssignal der Messeinheit (7) kann einerseits zur Anzeige der Kraft verwendet werden (8), wird andererseits aber einer Stufenkodierung (9) zugeführt. Diese Stufenkodierung erzeugt ein Triggersignal (10), welches zur Aufnahme der Bilddaten vom Video- oder HF-Ausgang (11) des Ultraschallgerätes verwendet wird. Eine mögliche Realisierung der Stufenkodierung basiert auf der Verwendung eines A/D-Wandlers mit nachgeschaltetem BCD/Dezimal-Dekoder. BCD/Dezimal-Dekoder des Typs 74x148 verfügen über ein Priority-Flag, welches das Anliegen einer Stufe kennzeichnet. Dieses Flag läßt sich günstig zur Triggierung der Aufnahmeeinheit (12) verwenden. Gleichzeitig kann die Höhe der Stufe, ebenfalls an den Rechner weitergegeben werden (15). Die aufgenommenen Daten werden dann im Computer mit bekannten Algorithmen weiterverarbeitet, und zur An-

zeige (13) getracht.

Zu Skizze 2 und Skizze 3: Endoskopische Schallsonde mit Dehnungssensor

Die Skizzen 2 und 3 enthalten Detailzeichnungen zur Anbringung der Dehnungssensoren am Sondenchaft, und erläutern die Kraftmessung nach dem Biegealkonzept. Die Sonde wird am Griff (5) gehalten und bei ihrer Verwendung mit der Spitze (1) in eine Körperöffnung (in der Regel transrektal oder transvaginal) eingeführt. Die Bildaufnahme erfolgt dabei üblicherweise senkrecht zur Ausrichtung des Sondenchaftes in der Ebene B, parallel zur Richtung der wirkenden Kraft F. Zu einer auf das Gewebe (7) wirkenden Kraft F resultiert eine Gegenkraft auf die Sonde, welches zu einer Biegung des Sondenchaftes (2) führt. Diese Biegung kann mit Hilfe der Dehnungssensoren (3) detektiert werden. Dehnungssensoren gibt es in verschiedenen Ausführungsformen und können unterschiedlich, d. h. einzeln, paarweise, oder vielfach, in vom Hersteller angegebenen Positionen und Verschalungen am Schaft der Sonde (4) befestigt werden. In der Skizze 3 wird die genaue Lage der zwei, in unserem Ausführungsbeispiel angebrachten Dehnungssensoren angedeutet.

Zu Skizze 4: Nicht-endoskopische Schallsonde mit hydrostatischem Drucksensor

Bei einer nicht-endoskopischen Sonde wird zur Kraftmessung eine wassergefüllte, schalldurchlässige Kappe (2) an der Schallwandler angebracht. Diese Kappe ist mit einer Metallscheibe (1) befestigt, und so abgedichtet, daß ein Auslaufen der Flüssigkeit verhindert wird. An einer Schlauchverlängerung (4), dessen Zugang zum Innenraum der Kappe ähnlich einem Fahrradventil ausgeführt werden kann (3), ist ein hydrostatischer Drucksensor (5) mit Zuleitungen (6) befestigt, der beliebig am Handgriff der Schallsonde (7) befestigt werden kann. Eine weitere Ausführungsform wäre, daß der Sensor direkt in die schalldurchlässige Kappe eingebaut wird. Eine auf den Wandler wirkende Kraft F führt zu einer Verformung der Kappe, und damit zu einer Veränderung des Druckes innerhalb des geschlossenen, mit Wasser gefüllten Systems. Diese Druckänderung kann mit Hilfe des Drucksensors gemessen werden.

Patentansprüche

- Ein Messsystem zur Bestimmung und Visualisierung von elastischen Gewebeeigenschaften mit diagnostischem Ultraschall, dadurch gekennzeichnet, daß die Kompression des Gewebes durch die Ultraschallsonde bewirkt wird und die von der Sonde auf das Gewebe ausgeübte Kraft gemessen, kontrolliert und dazu verwendet wird, Ultraschallbilder bzw. Bildsequenzen bei vorher festgelegten Kompressionsstufen aufzunehmen (Skizze 1).
- Ein Messsystem nach Anspruch 1, dadurch gekennzeichnet, daß bei entsprechendem gesteuerten Ultraschallwandler (starre Endoskopsonden) die Kraft auf das Gewebe mittels eines mit dem Schallwandler verbundenen Dehnungssensors nach dem Biegealkonzept gemessen wird (Skizzen 2 und 3).
- Ein Messsystem nach Anspruch 1, dadurch gekennzeichnet, daß die Kraft auf das Gewebe mittels eines mit dem Schallwandler verbundenen hydrostatischen Drucksensors gemessen wird (Skizze 4).
- Ein Messsystem nach Anspruch 1, dadurch gekennzeichnet, daß die Messung der Kraft auf das Gewebe

mit handelsüblichen Uruschallgeräten bzw. Sonden
mit geringfügiger Modifikation der Schalente er-
füllt kann, ohne gedruckte Veränderungen am (U-
uschallgerät vornehmen zu müssen.

Hierzu 3 Seiten/ Zeichnungen

3

10

15

20

25

30

35

40

45

50

55

60

65

- Leersseite -

tor, not being sensitive to phase changes, would still be more robust than the RF cross-correlation estimators. In fact, phantom experiments were used to show that the centroid estimator could generate quality elastograms at applied strains as high as 3% while the cross-correlation based elastograms are extremely noisy. Furthermore, simulation results showed that the spectral centroid shift method provided a jitter insensitive method of estimating the strain. Therefore, spectral strain estimation may be particularly useful for obtaining good elastograms in noisy jitter environments produced by unpredictable tissue and/or system motion. This may constitute a major advantage, since elastography might be practiced using the same clinical guidelines employed by ultrasound, i.e., using a hand-held transducer. In addition, the jitter resistance of the centroid estimator could make it suitable for use in intravascular elastography in vivo, a task that has not been demonstrated as feasible using cross-correlation techniques. Future investigations will involve theoretical study of the performance of spectral (i.e., frequency and shift and bandwidth) strain estimators as well as experimental verification of their jitter insensitivity.

[0083] The foregoing disclosure and description of the invention are illustrative and explanatory. Various changes in the size, shape, and materials, as well as in the details of the illustrative construction may be made without departing from the spirit of the invention.

What is claimed:

1. A method for measuring strain in a target body comprising:
 - a. acoustically coupling a transducer to the outer surface of a target body such that the path of a beam emitted from the transducer defines a transducer axis;
 - b. emitting first a pulse of ultrasound energy into the target body along the transducer axis;

- c. receiving a first reflected signal with the transducer;
 - d. storing the first reflected signal;
 - e. allowing the target to change dimensions along the axis defined by the transducer;
 - f. emitting a second pulse of ultrasound energy into the target body along the transducer axis;
 - g. receiving a second reflected signal with the transducer;
 - h. storing the second reflected signal;
 - i. selecting a portion of the first and second reflected signals;
 - j. computing the frequency spectrum of each of the selected portions of the first and second selected signals;
 - k. computing the shift between the computed spectra; and
 - l. normalizing the computed shift to one of the computed spectra.
2. The method of claim 1 wherein allowing the target to change dimensions is accomplished by applying a compressive force to the target.
 3. The method of claim 1 wherein allowing the target to change dimensions is accomplished by reducing a compressive force to the target.
 4. A method of claim 1 wherein computing the frequency spectrum of each of the selected portions of the first and second selected signals is accomplished using Fourier analysis.

* * * * *

United States

(19) Patent Application Publication (10) Pub. No.: US 2002/0010399 A1
 (12) Patent Application Publication (43) Pub. Date: Jan. 24, 2002
 Konofagou et al.

(54) POWER SPECTRAL-STRAIN ESTIMATORS IN ELASTOGRAPHY

(76) Inventors: Elissa Konofagou, Boston, MA (US);
 Jonathan Ophir, Houston, TX (US)

Correspondence Address:
 Richard T. Redino
 Duane, Morris & Hecksher LLP
 Suite 300
 One Greenway Plaza
 Houston, TX 77046 (US)

(21) Appl. No.: 09/810,958

(22) Filed: Mar. 16, 2001

Related U.S. Application Data

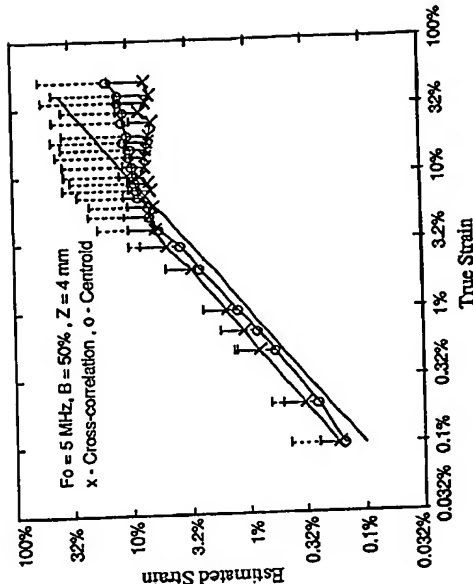
(63) Non-provisional of provisional application No.
 60/190,718, filed on Mar. 17, 2000.

Publication Classification

(51) Int. Cl.⁷ A61B 8/02
 (52) U.S. Cl. 600/449

ABSTRACT

Elastography can produce quality strain images in vitro and in vivo. Standard elastography uses a coherent cross-correlation technique to estimate tissue displacement and tissue strain using a subsequent gradient operator. While coherent estimation methods generally have the advantage of being highly accurate and precise, even relatively small undesired motions are likely to cause enough signal decorrelation to produce significant degradation of the elastogram. For elastography to become more universally practical in such applications as hand-held, intravascular and abdominal imaging, the limitations associated with coherent strain estimation methods that require tissue and system stability, must be overcome. In this paper, we propose the use of a spectral shift method that uses a centroid shift estimate to measure local strain directly. Furthermore, we also show theoretically that a spectral bandwidth method can also provide a direct strain estimation. We demonstrate that strain estimation using the spectral shift technique is moderately less precise but far more robust than the cross-correlation method. A theoretical analysis as well as simulations and experimental results are used to illustrate the properties associated with this method.



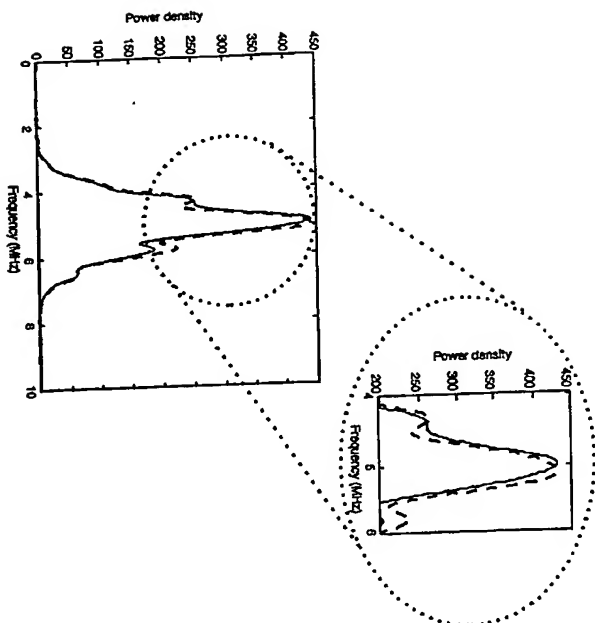


Figure 1

finite element analysis (FEA) commercial software (A1 FOR, Inc., Pittsburgh, Pa., USA). The simulated totally compressible and isotropic phantom contained a single inclusion three times larger than the homogeneous background (background modulus=21 MPa). All nodes were constrained to move solely in the axial direction, thereby avoiding decoherence in other directions. This motion model was therefore considered one-dimensional. The scatterers were normally distributed. The ultrasonic parameters were as follows: center frequency 5 MHz, 50% 6 dB bandwidth and 100 A-lines.

[0073] The strain estimation noise performance of the centroid estimator was compared to that of the standard elastographic cross-correlation-based strain estimator without motion compensation, i.e., global stretching. As explained in the introduction, motion compensation was not used, since the noise to which the robustness of the two estimators is tested is precisely the one due to axial motion.

[0074] FIG. 6 presents the elastograms obtained using both these methods along with the ideal elastogram (i.e., true strain image) for three different applied compressions. Note that at the low strain value of 1%, FIG. 6 (i), the elastogram generated using the cross-correlation algorithm implies the closest correspondence to the ideal elastogram. On the other hand, for larger applied strains (5% and 10%, FIG. 6 (ii) & (iii)), the cross-correlation algorithm fails to accurately estimate the strain, due to the increased signal decoherence errors (FIG. 6b (i) & (ii), respectively). In fact, at 5% applied compression part of the background is still visible, being three times larger than the background and, thus, experiencing a much lower strain allowing it to be depicted with a good signal-to-noise ratio. On the other hand, the elastogram generated using the spectral centroid method at 5% and 10 % compression (FIG. 6c (i) & (ii), respectively) illustrates the robustness associated with the centroid method.

[0075] In the next section, we present elastograms obtained using an elastographic experimental phantom. The experimental results provide a complete 3-D situation where axial, lateral and elevational signal decoherence are present, unlike the 1-D situation illustrated in this section.

[0076] Elastographic experimental results

[0077] The ultrasound system used for taking the data was a Diasonics Spectra II real-time scanner (Diasonics Inc., Santa Clara, Calif.) operating with dynamic receive focusing and a single transmit focus centered at a depth of 3 cm. The transducer used was a 5 MHz linear array (40 mm) with a 60% fractional bandwidth. The digitizer used is a Rbbit digitizer (Lectro Corp., Spring Valley, N.Y.) with a sampling rate of 48 MHz. The digitized data was collected from a 40x50 mm ROI consisting of 100 A-lines (starting at a depth of 5 mm under the transducer) centered around the transmit focus. The system also included a motion control system, and a compression device. A personal computer controlled the operation of the entire system.

[0078] A gelatin phantom (90x90x80 mm³) containing a cylindrical inclusion with a 20 mm diameter, positioned at the center of the phantom and three times stiffer than the background was used to compare the performance of the strain estimators. The phantom contains scatterers (graphic flakes) and was used to obtain RF scans before and after compression. A large compressor was used to simulate uniform stress conditions in the phantom. The phantom was lubricated on the top and bottom surfaces with corn-oil to

stimulate slip boundary conditions and was free on both lateral and elevational sides.

⁷The elastographic phantom was supplied courtesy of Dr. Timothy Hall (John et al. 1997).

[0079] Comparison of the estimation performance using coherent cross-correlation and centroid strain estimators is illustrated qualitatively using elastograms obtained at both low (0.5%) and high (5%) applied strains in FIG. 7. Note that coherent strain estimation provides the elastogram with the highest for the low compression of 0.5% (FIG. 7 (i)), when compared to the centroid method. However, for the large applied compression of 5% (FIG. 7 (ii)) the coherent strain estimator fails completely when compared to the spectral centroid method which produces a reasonable elastogram. In addition, averaging several elastograms obtained from independent pre- and post-compression data can be used to further improve the elastograms for the centroid method. However, averaging is not useful for the coherent cross-correlation strain estimator in this case since the RF signals are completely decohered producing (FIG. 7c (i)).

[0080] Two major differences can be observed between the 1-D simulation results and the experimental results: a) The mechanical artifacts for the 1-D simulation elastograms are along the top and bottom axes of the inclusion, when compared to the more complicated artifacts observed for the 3-D case; and b) the cross-correlation algorithm fails at relatively lower applied strains (3% instead of 5% or 10%) than in the simulation results due to lateral and elevational decohering motion involved. The centroid method yields similar results in both cases of low and high applied strains demonstrating its robustness in 3-D scenario as well. These results are comparable to what has been obtained with the iterative correction method and may indicate, despite its lower precision, a more computationally efficient as well as robust method of estimating axial strain.

[0081] The new concept described in this paper is based on the direct estimation of tissue strain from the relative frequency shift in the power spectrum. The estimator hereby presented, namely the centroid shift estimator, measures the shift by calculating the relative centroid shift resulting from the applied compression. This estimator has three major characteristics: it is a) direct and b) spectral, i.e., operates in the frequency domain. The direct strain estimation assures that no noise is added through the use of gradient operators, as is the case in time-shift based elastographic techniques. The spectral characteristic makes this method more robust since it is phase independent and, therefore, suffers less from motion-induced decoherence noise. Another estimator that is theoretically shown to provide a direct measure of strain is the resulting relative change of bandwidth in the power spectrum. The bandwidth parameter can also be used to eliminate the bias corrupting the centroid estimator.

[0082] In order to study the performance of the centroid estimator, we used a 1-D simulation model that allowed the scatterers to move solely in the axial direction. Preliminary results obtained with these 1-D simulations are used to demonstrate the robustness of the proposed method. Strain estimates as high as 10% are produced at a reasonably high signal-to-noise ratio while the standard cross-correlation-based elastographic method practically failed beyond the levels of 2%. The 1-D example was preferred to 2-D or 3-D simulations so that the performance of the method could be characterized independent of noise due to 2-D or 3-D motion. If the 2-D or 3-D scenario were used, the estimators would fail at lower strains, but the spectral centroid estima-

5

4 mm and the size of post-compression window was changed with strain in order to assure that the same tissue information was incorporated in both the pre- and post-compressed windows. The length of the data segment incurred the usual tradeoff in spectrum estimation. A larger window length improved the spectrum as long as the data was stationary. Moreover, it was recently shown that the overlap has a more significant impact on resolution than the window length. As a result, larger windows with high overlap can generally provide both a smoothing effect on the noise and high resolution for both the time-domain and spectral estimators. This effect, however, needs to be further investigated.

[0066] The power spectra calculation of the pre- and post-compressed RF segments was performed using a 25-point frequency smoothing window unless otherwise stated. The 25 point frequency smoothing window represents only 0.6% of the entire FR, and is a relative small window. Frequency smoothing is similar to using a moving-average window, however the averaging is performed on the complex spectrum to obtain an estimate of the power spectrum. Frequency smoothing allowed the use of a single pair of A-lines, similar to the strain estimation performed using the cross-correlation-based strain estimator. We use a 1024 point chirp Z-Transform to compute the spectrum which would correspond to a 4096 point FFT (since we use only one half of the spectrum, and only the region with a sufficient signal). The mean and standard deviation of the strain estimates were obtained by processing pre- and post-compression A-lines with a total length of 30 mm. The corresponding SNR (ratio of the mean of the estimated strain to its standard deviation) values were obtained using Monte Carlo simulations in MATLAB with 25 independent realizations for each strain value. The simulated Strain Filters were obtained by plotting the SNR estimates for the whole range of the applied tissue strains. The Strain Filter typically addresses the limitations of the ultrasound system (such as time-bandwidth product, center frequency and sonographic SNR) as well as the signal processing algorithms used to process the signals through the introduction of constraints in the attainable elastographic SNR, resolution, sensitivity and strain dynamic range.

[0067] The robustness of the strain estimators was also evaluated by introducing jitter errors in the scatterer positions before generating the post-compression signals. The jitter in the scatterer positions followed a normal distribution that varied randomly from zero to the maximum value of the jitter introduced. For the larger jitter values the scatterers could move out of the window of estimation. The strain estimation accuracy and precision for the coherent estimators were expected to deteriorate under these conditions since they depend on the relative motion of the scatterers themselves with compression. However, the centroid estimator, being incoherent, was expected to show strain estimation with a reasonable SNR, even at high jitter levels.

[0068] An example of the frequency shift on simulated spectra of entire A-lines (40 mm in length) is shown in FIG. 1 for the case of 1% applied strain. Comparison of the strain estimations using the coherent cross-correlation and centroid based algorithms are presented in FIGS. 2 and 3 for the 1-D simulations. The mean strain estimates and their standard deviation are presented in FIG. 2 and the respective simulated Strain Filters are presented in FIG. 3. The results in FIG. 2 illustrate that the strain estimates from both estimators

follow the theoretical curve (straight solid line at 45 degrees) for strains less than 5%, where the cross-correlation strain estimator begins to level off, and at 8% where the centroid strain estimator crosses the theoretical curve. Both estimators are biased with a small overestimation of the strain seen for strains lower than 5%. For larger strains, the centroid estimator underestimates the actual strain values with a larger bias in the estimated strain value. This bias in the strain estimation for the centroid estimator is at least partly due to the bandwidth broadening, as discussed in the theory section. The bias in the cross-correlation based strain estimator is due to the errors associated with tissue compression that corrupt the time-delay estimates. These bias errors can be reduced by temporally stretching the post-compression data. Overall, when compared to the standard elastographic coherent estimator, the centroid strain estimator provides a biased but more robust strain estimate.

[0069] In FIG. 3, the simulation Strain Filters for the two algorithms illustrate the noise performance of the estimators. Note that the coherent cross-correlation strain estimator provides accurate and precise strain estimates for strains less than 2%, since the variance increases rapidly beyond this strain value; however, for larger strains the performance deteriorates significantly. On the other hand, the centroid strain estimator, not being sensitive to phase, provides a robust strain estimate even at very large strains close to 30%. The SF for the centroid strain estimator indicates a reasonable SNR, for low tissue strains as well as an increase in the SNR, observed for larger strains where the cross-correlation strain estimator is limited by signal decorrelation errors. Due to its lower precision the centroid estimator works best at higher strains where the shift is greater and remains constant increases, as shown in FIG. 3. The simulations therefore show the robustness of the spectral centroid strain estimator to large applied strains and increased jitter, errors that are most likely to be encountered in hand-held or intravascular or abdominal elastography.

[0070] Next, we investigated the sensitivity of the cross-correlation and spectral strain estimator to variations in the scatterer positions caused due to axial jitter. The results are illustrated in FIGS. 4 and 5 for the cross-correlation and centroid strain estimators respectively. Note that the coherent cross-correlation-based strain estimator is more susceptible to jitter than the centroid strain estimator. The noise performance of the cross-correlation estimator drops by about 50% with an increase in the maximum value of the jitter by 50 ns. However, in the case of the centroid strain estimator the noise performance remains at the same high level, even at jitter magnitudes of 100 ns. The simulations, therefore, show the robustness of the spectral centroid strain estimator to large applied strains and increased jitter, errors that are most likely to be encountered in hand held or intravascular or abdominal elastography. The two following sections compare elastograms obtained with these two estimators in the case of a 1-D finite-element simulation and an experimental phantom.

[0071] Elastograms using simulated data

[0072] After testing the properties of the new estimator in the previous section, elastograms were generated for a simulated single inclusion phantom under uniform compression. For the calculation of the displacements, we used a

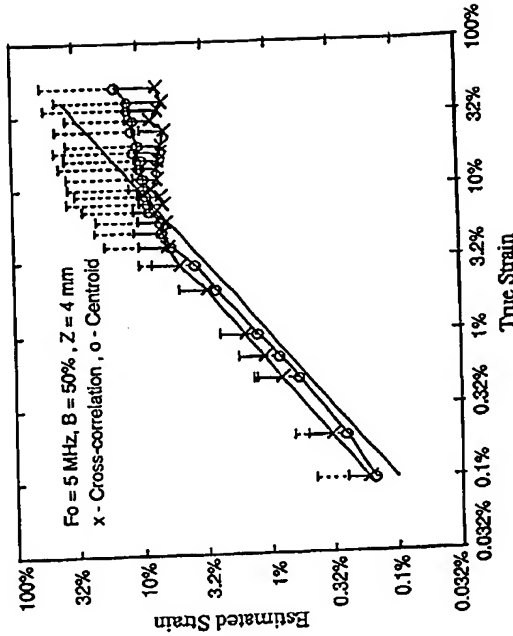


Figure 2

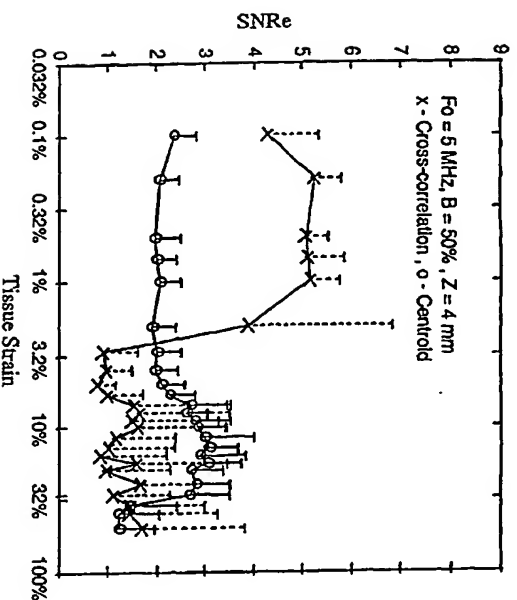


Figure 3

the centroid estimator. Otherwise, if R_c is infinite and/or if k_c is zero, constant A in Eq. (10) will always be zero regardless the strain.

[0043] For relatively larger strains, using the more general form of Eq. (3), Eq. (10) becomes

$$\frac{f_c - f_c'}{f_c} = A \sqrt{1 - \epsilon^2}$$

[0044] or, by solving for the strain,

$$\epsilon = \frac{f_c - f_c'}{f_c} \sqrt{1 + \frac{f_c}{A^2}} \quad (19)$$

[0045] which is a less straightforward, but still a direct way of estimating higher strains.

[0046] Eq. (16) is reminiscent of the well-known Doppler effect, according to which the ratio of the centroid shift to the center frequency may provide a reliable measure of velocity. According to Eq. (16), in the case of strain, a similar effect also occurs. Also, among others have shown how in broad-band Doppler the bandwidth of the resulting spectrum also changes with velocity and that the output RF Doppler spectrum is a frequency-shifted and compressed (or stretched) replica of the transmitted one. Similarly, in the case of strain measurement, that the following expression provides a direct estimation of strain:

$$\frac{f_c - f_c'}{f_c} = \epsilon \quad (20)$$

[0047] where ϵ are the post- and precompression bandwidths, respectively and k is a constant. So, strain, like velocity, introduces these two coupled effects of centroid shift and bandwidth variation in the power spectrum. Spectral broadening (i.e., in the case of compression) or contraction (i.e., in the case of tension) can introduce a bias in the measurement. A general expression is derived, linking the centroids f_c and f_c' (before and after compression, respectively), the pure frequency shift (i.e., in case the pre and postcompression spectra are identical, only centered at different frequencies separated by a shift), Δf , and a bias term p denoting the spectral broadening (or, compression) due to strain ϵ .

$$f_c - f_c' = \Delta f + p \quad (21)$$

where

$$p = B_c - B_c' \quad (22)$$

[0049] In order to estimate the strain without the bias associated with spectral broadening, the following equation can be used that results from Eqs. (10), (20), (21) and (22):

$$\Delta f - k_c' = \Delta f_c \quad (23)$$

[0050] and solving for strain, the unbiased estimator is given by

$$\epsilon = \frac{\Delta f}{\Delta f_c - \Delta f_c'} \quad (24)$$

[0051] However, Eq. (24) requires a bandwidth estimation and since the bandwidth estimator is not part of this study we use Eq. (16) as the strain estimator and show a bias with simulations, which is partly due to the previously described bias due to spectral broadening.

DESCRIPTION OF THE DRAWINGS

[0052] FIG. 1 is a graph of power density versus frequency.

[0053] FIG. 2 is a graph of estimated strain versus true strain.

[0054] FIG. 3 is a graph of signal to noise ratio versus tissue strain.

[0055] FIG. 4 is a graph of signal to noise ratio versus tissue strain.

[0056] FIG. 5 is a graph of signal to noise ratio versus tissue strain.

[0057] FIG. 6 (i) a-c are elastographs.

[0058] FIG. 7 (ii) a-c are elastographs.

[0059] FIG. 8 (iii) a-c are elastographs.

[0060] FIG. 7 comprises various elastographs.

[0061] FIG. 8 is a graph of power spectrum versus frequency.

[0062] 4. Description of the Preferred Embodiments

[0063] Simulation results using a 1-D scattering model is used in this section to illustrate the performance of the centroid strain estimator. Strain estimation using the centroid is also compared to the standard cross-correlation based algorithm.

[0064] Monte-Carlo simulations in MATLAB (Mathworks, Inc., Natick, Mass., USA) are used to generate pre- and post-compression RF signals for a 30 mm target segment and sampled at 48 MHz. The speed of sound in tissue was assumed to be constant at 1540 m/s. The PSF was simulated using a Gaussian modulated cosine pulse with a wave number of 200 1/m (5 MHz center frequency, 50% bandwidth), and a 0.2138 mm standard deviation (unbiased otherwise). The scattering function consisted of randomly distributed point scatterers following a uniform distribution with density of 40 scatterers/pulse-width in order to simulate Gaussian statistics. We assume that the uniformly distributed scatterers are of a sufficient number to generate an echo signal with circular Gaussian statistics. The PSF was convolved with the scattering function to obtain the pre-compression RF signal. The post-compression signals were generated after applying a uniform compression of the point scatterers, and convolving the compressed point scatterers with the original PSF.

[0065] Spectral strain estimation (following Eqs. 16 and 11) was performed using pre- and postcompressed power spectra of windowed RF signals. The signal length equaled

3

similar result is found later (Eq. 16) using the spectrum of the received signal. In the section below, we use Eq. (10) as a guide in the formulation of the new estimator.

[0027] Effect of strain on the spectrum of the received signal

[0028] The centroid of the power spectrum of the received signal is defined as follows

$$f_c = \frac{\int_0^\infty f R(f) df}{\int_0^\infty R(f) df} \quad (11)$$

[0029] The centroid estimate for the precompression power spectrum is given by:

$$f_{c1} = \frac{\int_0^\infty f L_p(f) df}{\int_0^\infty L_p(f) df} \quad (12)$$

[0030] In a similar manner we can derive the expression for the centroid of the post-compression power spectrum by replacing L_p and L_s in Eq. (9) by their corresponding parameters in the post-compression power spectrum, i.e., λk and

$$\frac{L_s}{\sigma}$$

[0031] (as indicated from Eq. 7) to obtain:

$$f_{c2} = \frac{\int_0^\infty f L_s(f) df}{\int_0^\infty L_s(f) df} \quad (13)$$

[0032] Note that the PSF parameters remain unchanged. Since both centroids depend on the center frequencies and bandwidths of the scattering function and the PSF and by consulting Eq. (10), we normalize this effect by using the following ratio as a candidate strain estimator:

$$\frac{f_{c2} - f_{c1}}{f_{c1}} = \frac{\frac{\int_0^\infty f L_s(f) df}{\int_0^\infty L_s(f) df} - \frac{\int_0^\infty f L_p(f) df}{\int_0^\infty L_p(f) df}}{\frac{\int_0^\infty f L_p(f) df}{\int_0^\infty L_p(f) df}} \quad (14)$$

[0033] The parameters L_p and L_s are related to B_p and B_s , the equivalent noise spectral bandwidths for the scattering and PSF spectra, through

$$B_p = \frac{1}{2\sqrt{\pi} L_p} \text{ and } B_s = \frac{1}{2\sqrt{\pi} L_s}$$

[0034] respectively.

[0035] However, the PSF bandwidth is typically much smaller than the bandwidth of the scattering function, i.e., $B_p \gg B_s$, thereby, $L_p \ll L_s$ and, therefore, $\frac{1}{L_p} \gg \frac{1}{L_s}$. After cancellation of common terms in the numerator and denominator of Eq. (14), we obtain

$$\frac{f_{c2} - f_{c1}}{f_{c1}} = \frac{\frac{\int_0^\infty f L_s(f) df}{\int_0^\infty L_s(f) df} - \frac{\int_0^\infty f L_p(f) df}{\int_0^\infty L_p(f) df}}{\frac{\int_0^\infty f L_p(f) df}{\int_0^\infty L_p(f) df}} \approx \frac{\int_0^\infty f L_s(f) df}{\int_0^\infty L_s(f) df} - 1 \quad (15)$$

[0036] or, from the small strain approximation case of Eq. (3) (i.e., in mathematical terms, for strains less than 10%),

$$\frac{f_{c2} - f_{c1}}{f_{c1}} \approx \lambda A \quad (16)$$

[0037] where λ is given by

$$\lambda = \frac{1}{\frac{L_p}{L_s} + 1} \approx \frac{L_p}{L_s} \quad (17)$$

$$\lambda = \frac{L_p B_p^2}{L_s B_s^2} \quad (18)$$

[0038] Inspection of Eq. (16) leads to the following interesting observations:

[0039] The relative spectral centroid shift can be used as a direct strain estimator. We can also observe a direct analogy between the classic definition of strain (Eq. (9)) and the estimator of Eq. (16), which establishes this method as a simple and straight-forward way of estimating the strain.

[0040] When the strain is positive (or, compressive), a frequency upshift occurs, i.e., $f_{c2} - f_{c1} > 0$. Conversely, a tensile (or, negative) strain results in a frequency downshift, i.e., $f_{c2} - f_{c1} < 0$. Therefore, the estimator of Eq. (16) provides directly not only the magnitude of the strain but also its sign.

[0041] Since constant λ is independent of the strain, it will introduce a uniform bias on the resulting elastogram. This should not affect the resulting elastogram, since the latter depicts relative values of strain. The reader should note that the effect of local bandwidth variations is ignored.

[0042] The scattering spectrum must be a bandpass and bandlimited spectrum in order to estimate the strain using

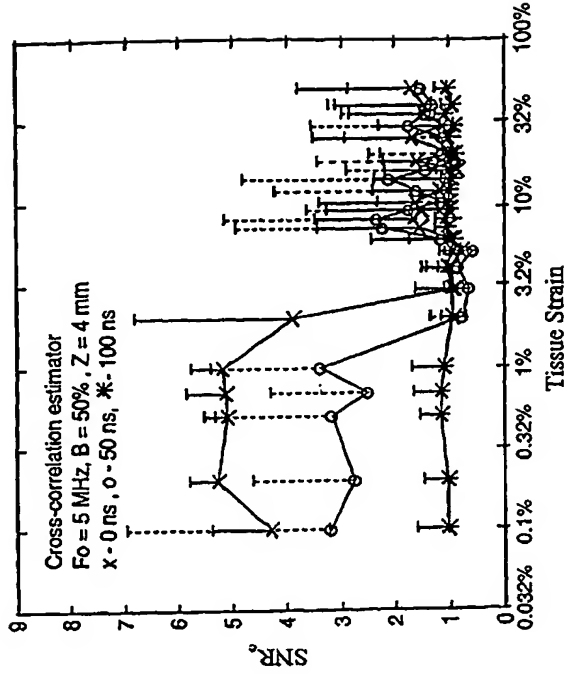


Figure 4

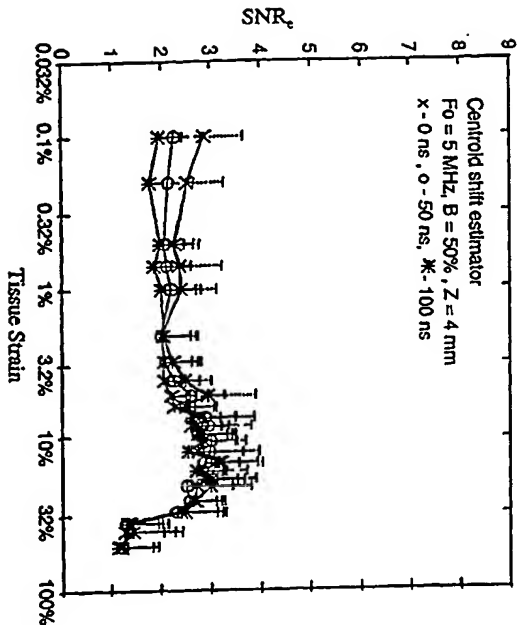


Figure 5

tions that deal with the development of alternative shift estimators as well as bandwidth estimators will not be reported in this study.

[0012] The spectral centroid has been widely used in estimating the Doppler shift, attenuation and backscattering. The theory underlying the use of centroid strain estimators is presented in the next section. One-dimensional (1-D), instead of two-dimensional (2-D), motion simulations are used in order to more accurately study the performance of the estimator, i.e., independent of the effect of signal decorrelation in two dimensions that complicates the measurements. Simulation results in 1-D illustrate the insensitivity of the centroid strain estimator to signal decorrelation effects. It is important to note that, as mentioned earlier, decorrelation can be due to several sources. For the purpose of this paper, we consider solely the axial decorrelation effect in this 1-D model. We, thus, assume that the robustness demonstrated by the spectral estimator vis-a-vis this effect is a more general property that can be further applied at other decorrelation scenarios. For example, it is shown in the results section how the spectral method is indeed more immune to jitter, another source of decorrelation. The ultrasonograms obtained using these simulations as well as phantom experiments illustrate the robustness of the spectral centroid strain estimator. The properties of the new estimator are discussed and summarized in the Conclusion section.

[0013] In this section we show analytically that for Gaussian echo spectra, the relative spectral shift is a direct measure of tissue strain. We also show the relative bandwidth variation can also be used as a direct strain estimator.

[0014] Signal and noise model.

[0015] The pre- and post-compression echo signals are given as follows:

$$r_1(t) = h(z) e^{j2\pi f_0 t} + n_1(t) \quad (1)$$

$$r_2(t) = h(z) e^{j2\pi f_0 t} + n_2(t) \quad (2)$$

[0016] where z is a spatial variable, $f_1(t)$ and $f_2(t)$ are the received RF signals before and after compression, respectively, $h(z)$ is the impulse response of the ultrasound system or point-spread function (PSF), $e^{j2\pi f_0 t}$ is the scattering function, $n_1(t)$ and $n_2(t)$ are independent zero-mean white noise sources and α is the compression coefficient (or, strain factor) linked to strain s through

$$\alpha = \frac{1}{1-s} \approx 1+s \quad (3)$$

[0017] The approximation holds for $s \ll 1$, where the strain s for a one-dimensional homogeneous target is typically defined in mechanics by

$$s = \frac{L_0 - L}{L_0} \quad (4)$$

[0018] where L_0 and L are the pre- and postcompressed axial dimensions of the target. From Eq. (4) the reader should note that positive strain denotes compression (and $s > 1$) while negative strain denotes tension (and $s < -1$). The

US 2002/0010399 A1

2

Jan. 24, 2002

reader should note that throughout this paper the subscripts 1 and 2 denote pre- and postcompression parameters, respectively.

[0019] Assuming that $h(z)$ and $e^{j2\pi f_0 t}$ in Eqs. (1) and (2) can be described by their autocorrelation functions that may be modeled by modulated Gaussian functions, we obtain

$$R_1(t) = \frac{1}{\sqrt{2\pi} L_0} \exp(-t^2/2L_0^2) \exp(j2\pi f_0 t) \quad (5)$$

$$\text{and} \quad (6)$$

$$R_2(t) = \frac{1}{\sqrt{2\pi} L} \exp(-t^2/2L^2) \exp(j2\pi f_0 t) \quad (6)$$

[0020] and

[0021] where L_0 and L are the resolution lengths of the PSF and of the scattering function, respectively, L_0 is the central spatial frequency of the PSF, and L is the central spatial frequency of the scattering function.

[0022] The one-sided power spectra of the pre- and post-compression RF signals (positive frequencies) are given respectively by

$$R_1(f) = \frac{1}{2} \exp\left(-\frac{1}{2}(f-f_0)^2 L_0^2 + j(f-f_0)^2 L_0^2\right) + N_1(f) \quad (7)$$

$$R_2(f) = \frac{1}{2} \exp\left(-\frac{1}{2}(f-f_0)^2 L^2 + j(f-f_0)^2 L^2\right) + N_2(f) \quad (8)$$

[0023] where $N_1(f)$ and $N_2(f)$ are independent power spectra of zero-mean white noise processes, i.e.,

$$\langle N_1(t) N_2(t) \rangle = \langle N_1(t) \rangle \langle N_2(t) \rangle = 0.$$

[0024] A brief observation of Eqs. (7) and (8) reveals the centroid shift in the scattering spectrum resulting from the compression. In other words, if f_1 and f_2 are the center frequencies of the scattering spectrum before and after compression, respectively, and assuming that the speed of sound in the tissue remains constant, from Eqs. (7) and (8) we have

$$f_2 - f_1 = \frac{c}{2L_0} (L_0 - L) \quad (9)$$

$$= (1-s)/L_0.$$

[0025] or, from Eq. (3)

$$\frac{f_2 - f_1}{f_1} = s \quad (10)$$

[0026] So, the relative centroid shift in the scattering function spectrum constitutes a direct strain estimator. A

POWER SPECTRAL STRAIN ESTIMATORS IN ELASTOGRAPHY

BACKGROUND OF THE INVENTION

- [0001] 1. Field of the Invention
- [0002] The present invention relates to a method of measuring strain in a target body, using the transmission, reception, processing and normalization of ultrasound signals.
- [0003] 2. Description of the Prior Art
- [0004] Imaging of elastic parameters of soft tissue has developed into a new tool for diagnosis of disease. Current estimators of tissue motion, include a time-domain cross-correlation based speckle tracking algorithm, and a Fourier based speckle phase-tracking technique. These techniques are coherent estimation techniques, i.e., these methods are sensitive to phase variations. The coherent estimation techniques generally have the advantage of being highly precise. Strain Filter (SF) analysis has shown, however, that they are not very robust in the presence of even a small amount of decorrelation between the pre- and post-compression signals. The term robustness has been used in statistical analysis to denote the good performance of statistical tests, i.e., the homogeneity of the variance calculation, even if the data deviates from theoretical requirements. By equivalence in elastography, robustness denotes the consistently good performance of the estimator even at high decorrelation noise, i.e., keeping the variance of estimation at a relatively constant and low level at a large range of noise levels.
- [0005] The term decorrelation as used herein, is defined as the loss of full correlation between the pre- and post-compressed windowed signal segments. Therefore, decorrelation may be encountered due to many sources, such as intravascular motion, undesired lateral or elevational motion, jitter (i.e., any cause of misregistration between the pre- and post-compressed A-line segments), unstable mechanical setup, etc. The main idea in this study is to introduce a new estimator that is more immune to decorrelation compared to other estimators.
- [0006] 3. Summary of the Invention
- [0007] The tissue strain estimator is a spectral estimator that estimates strain directly. Since the proposed estimator uses the power spectrum, it is incoherent, i.e., it does not use the phase of the signal. Previously reported incoherent methods include optical flow speckle tracking, envelope cross-correlation, and spectral chirp z-transform techniques. Generally, incoherent methods may be less precise but significantly more robust. For example, we have demonstrated this property for the case of time-delay estimation using the envelope of echo-signals. This may be a significant advantage where elastography is to be practiced in situations involving (1) undesired scanning motion, such as the case of using an unstable handheld transducer and/or (2) undesired tissue motion, such as abdominal or intravascular elastography. This property of the estimator is demonstrated later in this paper in the simulation results section through testing of its immunity to noise caused by jitter.
- [0008] The main idea behind a spectral strain approach is based on the Fourier scaling property, which implies that a compression or expansion of the time-domain signal should lead to an expansion or compression of its power spectrum,

respectively. One of the most well known and thoroughly studied spectral motion effects is the Doppler shift, which typically links the frequency shift to the scatterer velocity between emissions. Velocities towards the transducer result in a positive frequency shift, while the opposite is true for scatterers that move away from the transducer. However, since the scatterers within a given resolution length do not move at the same velocities, a spectrum of Doppler frequencies is observed. Therefore, initially in ultrasound, the methods of velocity estimation for the measurement of blood flow mainly operated in the frequency domain, otherwise known as spectrum analysis techniques and measured the mean velocity of scatterers across the vessel lumen (indicative of the volumetric flow rate) by estimating the mean frequency of the power spectrum. Despite the success of these techniques even in vivo vessels, detection of the Doppler frequency shift, which is typically on the order of 1 kHz, is not possible for pulsed instruments, since the downshift in frequency due to attenuation (on the order of 10-100 kHz) is expected to dominate over the Doppler shift. Since in elastography the pre- and post-compressed segments are approximately identical depths, the attenuation effect on the two spectra is assumed to be identical and cancelled out when the two spectra are compared.

[0009] Strain estimation using spectral methods depends on the subsequent change in the scatterer statistics. Spectral methods typically link one or more signal parameters to the change in mean scatterer spacing. One prior art relates the relative change in the mean scatterer spacing to the strain incurred during a cardiac cycle. This method assumes the presence of underlying scatterer periodicities. Despite the fact that this has also been demonstrated to work in vivo intravascular applications, the main assumptions of regular spacing of periodicities may not hold for most tissues. In contrast, as shown in the theory section, the spectral methods mentioned in this paper make no assumptions regarding the composition of the tissue scatterers.

[0010] Typically in elastography time-domain techniques are used that involve the computation of the time-delay to estimate the displacement following an applied compression, and the estimation of strain by applying gradient operations on the previously obtained time-delay estimates. As mentioned earlier, an important advantage associated with these spectral methods as well as other estimators, such as the adaptive stretching estimator, is that they can be used to estimate strain directly, i.e., without involving the use of noisy gradient operators. In the latter case, the gradient operation introduces additional amplification of the noise into the strain estimation process, thus degrading the strain estimates. Furthermore, similar to the adaptive stretching estimator, only one estimation window is needed, for both the magnitude and the sign of the strain to be estimated.

[0011] As shown later in the theory section, spectral estimators can be divided into two main groups: a) the spectral shift methods and b) the spectral bandwidth methods. Despite the fact that we develop expressions that show direct strain estimation in both cases, in this paper we focus primarily on a spectral shift method; we estimate the relative shift in the spectral centroid caused by compressive or tensile tissue strain. Therefore, throughout this paper this new estimator is referred to as the centroid strain estimator, centroid estimator or centroid method. Current investiga-

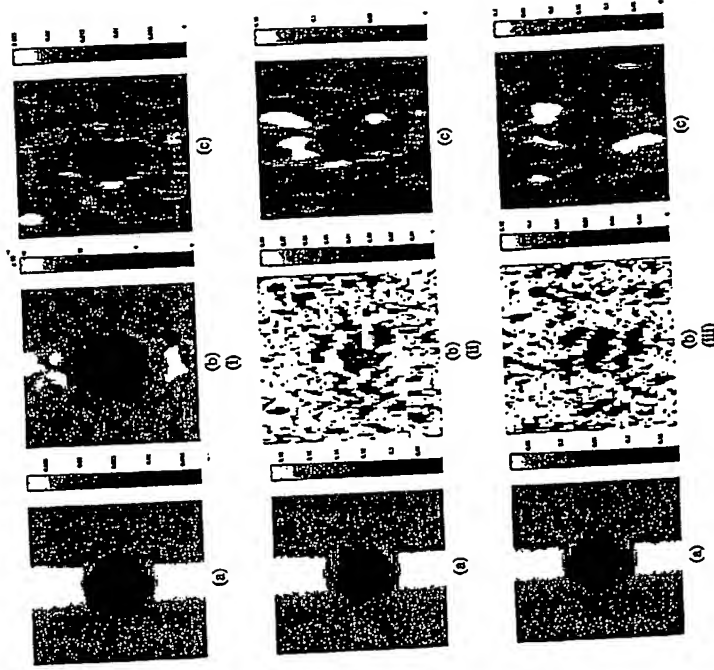


Figure 6

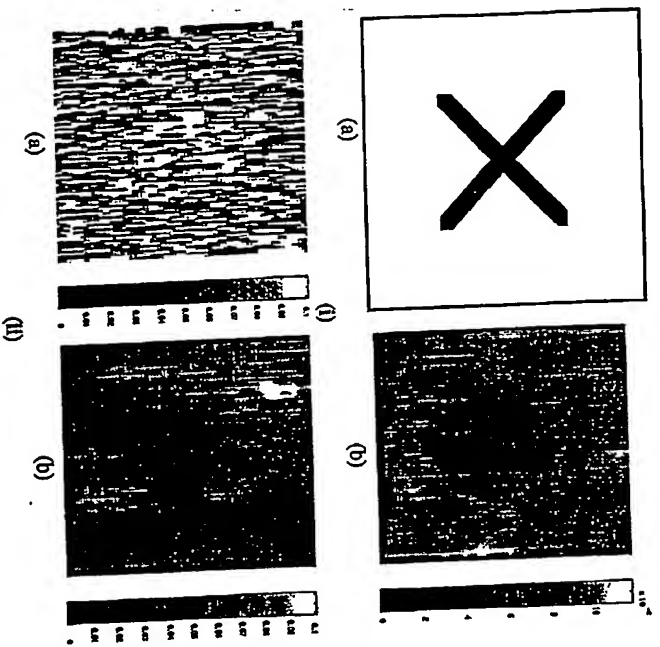


Figure 7

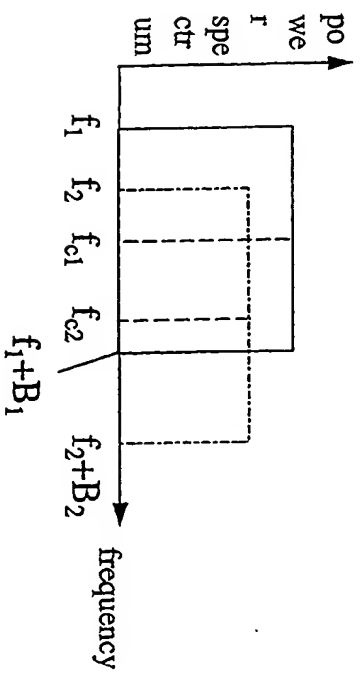


Figure B1

13

(g) coordinating said transmissions and detections such that the signal travel times between transmitters and detectors for the two transducers are about equal, and (h) performing characterization measurements based upon said detected reflection signals.

15. A method of obtaining ultrasonic echo data from a target body for tissue characterization measurement which comprises:

- (a) sequentially coupling and transmitting a separate pulse of ultrasonic energy into a target body from each one of a plurality of matched ultrasonic transducers which are sequentially placed in, and energized to transmit their respective pulses from, axially staggered positions along a common pulse transmission axis;
- (b) detecting a separate echo signal from the target body for each transmitted pulse such that the echo signals emanate from regions within the tissue

14

which are axially staggered along said pulse transmission axis in a relation corresponding to the axial stagger of their respective transducers along said pulse transmission axis and (c) performing characterization measurements based upon said detected echo signals.

16. The method of claim 15 comprising 4 to 6 matched ultrasonic transducers.

17. The method of claim 15, which further comprises, performing steps (a) and (b) along a plurality of spaced transmission axes.

18. The method of claim 11, wherein said characterization measurement performing step comprises obtaining the attenuation coefficient of the target body by the log spectral difference method.

19. The method of claim 18 in which adjacent said axes are spaced sufficiently from each other to be non-correlated.

• • • • •

20

25

30

35

40

45

50

55

60

65

United States Patent [19]

Ophir

[11] Patent Number: 4,993,416

[45] Date of Patent: Feb. 19, 1991

[54] SYSTEM FOR ULTRASONIC PAN FOCAL IMAGING AND AXIAL BEAM TRANSLATION

[73] Inventor: Jonathan Ophir, Houston, Tex.
[73] Assignee: Board of Regents The University of Texas System, Austin, Tex.

[21] Appl. No.: 343,405

[22] Filed: Apr. 25, 1989

[51] Int. Cl.⁷ A61B 8/00

[52] U.S. Cl. 128/660.06; 73/599; 128/660.09

[53] Field of Search 128/660.1; 73/633, 639, 599

[56] References Cited

U.S. PATENT DOCUMENTS

2,946,904	7/1960	Reant	310/12
4,177,679	12/1979	Soldner	73/625
4,242,913	1/1981	Merrich et al.	73/626
4,247,767	9/1981	Kret	128/660.09 X
4,294,119	10/1981	Soldner	73/625
4,324,160	4/1982	Adit	73/626
4,353,645	7/1982	Lee	73/626
4,389,893	6/1983	Ophir et al.	73/599
4,402,223	9/1983	Neumann, Jr. et al.	73/625
4,403,569	9/1983	Kret	73/625
4,413,371	2/1984	McAuland	128/660
4,452,084	6/1984	Tanner	73/609

OTHER PUBLICATIONS

Elimination of Diffraction Error in Acoustic Attenuation Estimation Via Axial Beam Translation, Ultrasonic Imaging, vol. 10, pp. 139-152 (1988), by Ophir and Mithra.

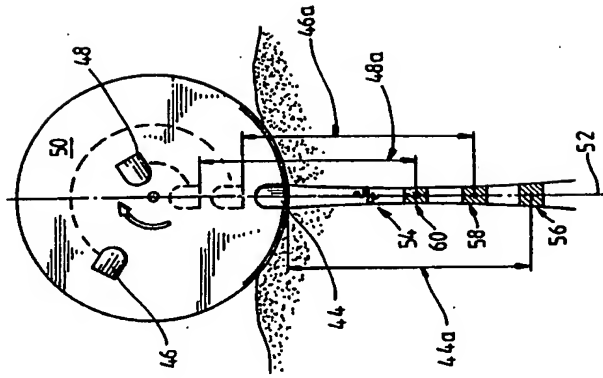
Primary Examiner—Francis Javoraki

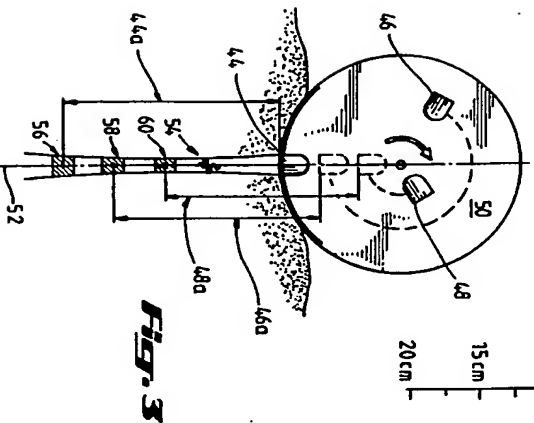
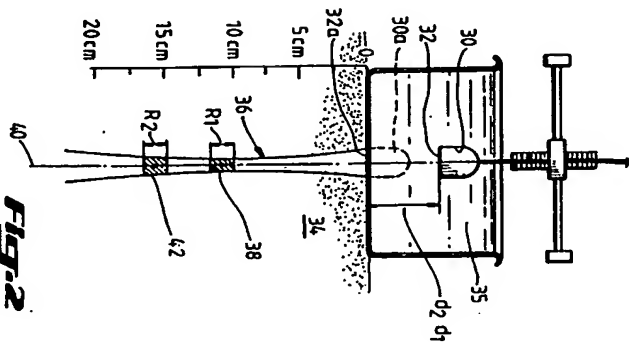
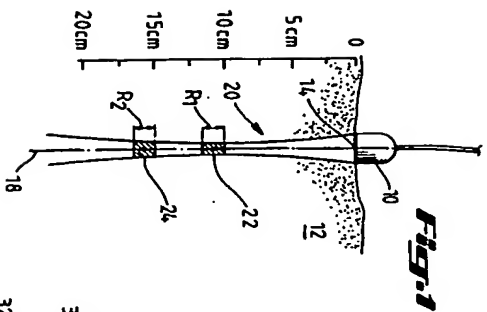
Attorney, Agent, or Firm—Arnold, White & Durkee

[57] ABSTRACT

The present invention provides a novel method and apparatus which allows concomitant imaging and rapid axial beam translation measurements used to calculate the attenuation characteristics of a target body. The present invention employs an ultrasonic scanner which contains a plurality of matched transducer elements. These elements are staggered on a mechanism which sequentially places each transducer opposite an acoustic window at axially spaced positions along a common axis. The present invention also enables axial beam translation techniques to be adapted to current ultrasonic imaging systems.

19 Claims, 4 Drawing Sheets





11

4,993,416

12

7. Optimize the data from step 6 to obtain the frequency band width that provides the best linear regression with frequency using a standard deviation parameter; and
 8. Compute the attenuation coefficient.
- Although the invention has been described with a certain degree of particularity, it is to be understood that the above description has been only by way of example. Numerous other changes will be apparent to those reading the specification without departing from the spirit and scope of the invention as claimed.
- What is claimed is:
1. Apparatus for tissue characterization measurement of a target body comprising:
 - (a) a plurality of matched ultrasonic transducers;
 - (b) a moveable mounting member adapted to mount the transducers in a spaced array such that movement of the mounting member sequentially positions the transducers in an axially staggered pattern along one or more common ultrasonic radiation axes to transmit and receive ultrasonic signals to and from the target body along the one or more common ultrasonic radiation axes up; and
 - (c) means coupled to said matched transducers for performing tissue characterization measurements by using said received ultrasonic signals.
 2. The apparatus of claim 1 wherein said mounting member sequentially positions the transducers along a plurality of common ultrasonic radiation axes.
 3. The apparatus of claim 2 comprising four to six 30 matched transducers.
 4. Apparatus for ultrasonic tissue characterization measurement of a target body comprising:
 - (a) a plurality of matched ultrasonic transducers, each of said transducers having an ultrasonic aperture;
 - (b) a moveable mounting member adapted to mount the transducers in a spaced array such that movement of the mounting member sequentially positions the transducers in an axially staggered pattern along one or more common ultrasonic radiation axes to transmit ultrasonic signals to the target body along the one or more common ultrasonic radiation axes;
 - (c) a range gate operable to detect a separate ultrasonic echo signal originating from said target body 45 in response to each transmitted signal wherein: (1) the detected echo signals emanate from regions within the target body which are axially staggered along said radiation axes in a relation corresponding to the axial stagger pattern of the transducers along said axis; and (2) the distances between each of said regions and the ultrasonic apertures of their respective transducers are about equal;
 - (d) means coupled to said matched transducers for performing tissue characterization measurements by using said received ultrasonic signals.
 5. The apparatus of claim 2 wherein said mounting member sequentially positions the transducers along a plurality of common ultrasonic radiation axes.
 6. The apparatus of claim 5 comprising four to six 60 matched transducers.
 7. Apparatus for ultrasonic characterization measurement of a target body comprising:
 - (a) a sealed housing adapted to contain an acoustic coupling fluid and having an acoustically transparent window disposed on the periphery;
 - (b) a disk disposed inside said housing and rotatably coupled to the housing;
 - (c) a plurality of matched transducers mounted to face radially outward on the disk in a spirally staggered pattern such that rotation of the disk sequentially and sequentially places said transducers across said window at axially spaced positions along one or more common ultrasonic radiation axes; and
 - (d) means coupled to said matched transducers for performing tissue characterization measurement.
 8. The apparatus of claim 7 comprising 4 to 6 matched transducers.
 9. The apparatus of claim 8 wherein said transducers are focused transducers.
 10. The apparatus of claim 5 wherein said mounting member sequentially positions the transducers along a plurality of common ultrasonic radiation axes.
 11. An apparatus for ultrasonic analysis of a target body comprising:
 - (a) a housing adapted to make contact with said body and to contain an acoustic coupling fluid;
 - (b) a mounting member mounted within the housing in rotatable relation thereto such that rotation of the mounting member causes points along the periphery of the mounting member to travel past the portion of the housing which makes contact with said target body;
 - (c) a plurality of matched ultrasonic transducers mounted on the mounting member in a pattern such that movement of the mounting member sequentially and sequentially positions each transducer adjacent the contact between the housing and the body and spaced along a common ultrasonic radiation axis extending through the contact into the body; and
 - (d) circuitry operable to separately activate each transducer when adjacent said contact so as to (1) transmit ultrasonic energy into the body and thereafter (2) receive a reflection of said energy from a region within the body such that the travel times of the energy between the transducers and their respective reflective regions within the body are about equal.
 12. The apparatus of claim 11 wherein the transducers are mounted in a spiral pattern on the moveable member.
 13. The apparatus of claim 6 which further comprises an acoustic window located in the portion of the housing which is adapted to contact the body.
 14. A method of performing an ultrasonic characterization measurement of a target body using a plurality of ultrasonic transducers which comprises:
 - (a) optically coupling a first ultrasonic transducer to a target body to transmit and receive ultrasonic signals to and from the body along a radiation axis;
 - (b) transmitting an ultrasonic signal from the first transducer along said radiation axis into the body;
 - (c) detecting reflection signals of the transmitted signal reflected from the body during a selected time interval following the transmission of the transmitted signal;
 - (d) decoupling and moving the first ultrasonic transducer away from its position on said radiation axis;
 - (e) moving a second transducer on to said radiation axis at a position axially spaced from the position occupied by the first transducer;
 - (f) repeating steps (a) through (d) for the second transducer;

4,993,416

gated strips 76a et seq. consist of a series of range gated regions such as 92. The number and location of these regions corresponds to the number of axes along which a transducer is pulsed as it sweeps the acoustic window. The number of times a transducer is pulsed corresponds to the radial scan line or a-line density. An a-line is the echo sequence corresponding to an ultrasound pulse as it propagates along a fixed axis through the target 95. The desired a-line density is based on considerations of adequate imaging and depth of penetration, and may be, for example, 170 a-lines per $\pi/3$ sector angle 99 for a depth of penetration of 20 centimeters. These figures, combined with the average speed of sound in tissue of 1540 meters per second, result in a sweep time per $\pi/3$ sector angle 99 of 45 milliseconds, or about 0.27 seconds for one revolution of disk 62. This allows a frame rate of approximately four frames per second. This frame rate, combined with hand-held contact scanning allows convenient imaging and attenuation estimation with ABT.

Continuing in FIG. 5, as transducer 76 sweeps acoustic window 64, it is activated approximately 170 times along 170 axes and acquires echoes corresponding to 170 regions (temporal windows) to form strip 76a. For example, an acoustic pulse will propagate within a particular beam having an axis 96. An echo signal which corresponds to region 92 is acquired from the a-line propagating along axis 96 using a range gate. As each successive transducer sweeps the acoustic window, each will be pulsed along the same axis, including 96, and acquire echo signals from its respective range gated strip, including 76a et seq. The data from the acquired signals may be combined to generate an extended focus image or may be used for attenuation estimations. Because of the transducer stagger pattern, each range gated strip is at a constant distance from its respective transducer aperture.

By acquiring approximately 170 echo sequences (a-lines) from the extended focus sector 98, the apparatus of FIG. 5 may obtain good quality images. However, in order to obtain a good measurement of the attenuation characteristics, the echo sequences used are advantageously "uncorrelated". A "correlated" a-line represents a non-statistically independent echo sequence. For example, at a range of 100 millimeters, 170 echo sequences across the $\pi/3$ sector angle correspond roughly to two a-lines per millimeter, and thus would be considered highly "correlated". This means that about only 1 out of 10 echo sequences should typically be used for attenuation estimation, or about 17 echo sequences per frame.

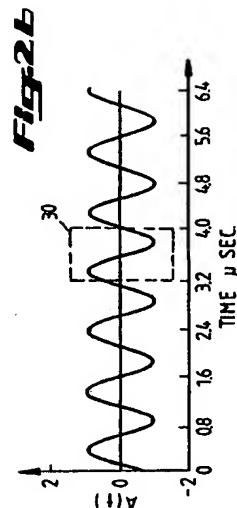
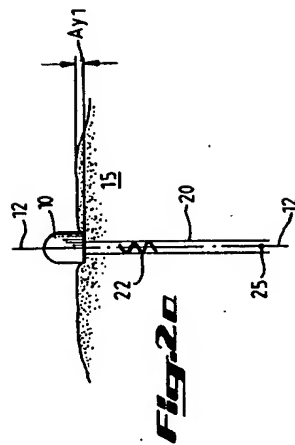
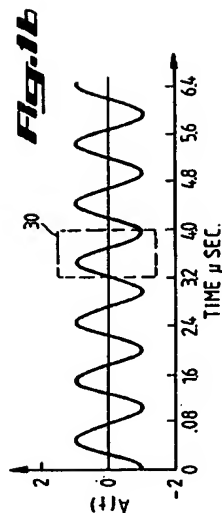
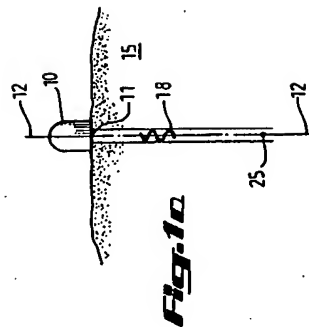
Typically, about 250 independent echo sequences may be acquired for an attenuation estimation. Conveniently, the a-lines may be acquired from multiple "uncorrelated" planes or frames. Therefore, the use of the scanning head in vivo may involve rocking the scanner from side to side over an angle of $\pi/4$ or so, and acquiring data from about 10 "uncorrelated" frames. If the device generates approximately 4 frames per second, rocking of the transducer will be accomplished in about 2.5 seconds. During the first frame, all 170 echo sequences (each comprising 6 segments acquired by the axially staggered transducers) may be digitized at a 25 MHz sampling rate and stored in half of the data acquisition system 116 in FIG. 6. During the second frame the echo sequences may be stored in the other half of the data acquisition system 116, while the data from the first frame is transferred to the computer 130.

10

Referring to FIG. 6, a representative block diagram of a system implementing the present invention is exemplified. The ABT scanning head 100 is driven by a 1024 step/revolution stepper motor 106, whose speed is controlled by a precision 3.9 KHz pulse repetition frequency ("PRF") clock 102, derived from a higher frequency 2 MHz master clock 104. An optical shaft encoder 108 is connected to the stepper motor 106 and provides absolute shaft angle information with 11 bit accuracy. The three most significant bits may serve as sector identifiers. The remaining bits may be used to code the individual echo sequences or a-lines. As the scanning head turns, the transducer multiplexer 110 sequentially selects one of the six transducers which is driven by the transmitter 112. Both the transmitter and the time-gain-compensation ("TGC") circuit 114 are driven from the 3.9 KHz PRF clock 102. The TGC or depth-compensation circuit amplifies echo signals in proportion to their transit time to compensate for signal attenuation. This allows for improved images on the display 118 and complete digitization of signals when fed into the data acquisition and storage system 116. A range gate 120 provides a write-enable signal to the digital scan converter ("DSC") 122 which allows pixels to be modulated on the display 118 corresponding to their respective range gated strips. The signal intended for imaging is fed into the demodulator 124 and then fed to the DSC 122. Position signals to the DSC 122 are provided by a dual x-y programmable-read-only-memory ("PROM") 126 which is strobed by the 2 MHz clock 104. The PROM generates a sequence of pre-programmed x-y addresses at a rate of 2 MHz. These addresses are converted to analog (position) signals and fed to the DSC 122. The DSC may operate in gated survey mode, such that individual sequential range gated strips in the image are updated, corresponding to the transducer with the appropriate focal distance which is swept across the acoustic window.

The ABT section of the exemplified apparatus involves eight bit digitization of the radio frequency ("RF") signal at 25-30 MHz via a data acquisition and storage system 116, and the TGC voltage at 25-30 KHz. These signals are later combined in software to calculate the absolute magnitude of the echo spectra. The output of the analog-digital converter 128 is communicated to the microcomputer 130 through the IEEE-488 bus 132. Using a six transducer scanner, the software for computing the attenuation coefficient may comprise, for example, the following steps:

1. Acquire 170 a-lines and divide into 6 segments (range gated strips) corresponding to 6 depths of observation within the target body;
2. Compute the average power spectrum for each depth by averaging the squared fast Fourier transform for all echoes in each segment over all a-lines;
3. Perform spectral smoothing by windowing the autocorrelation function of the averaged spectra obtained in step 2 above and re Fourier transforming to obtain a smoothed power spectrum;
4. Convert the power spectra of step 3 to units of dB (log of power spectrum);
5. Perform linear regression with respect to each depth of observation for all frequencies in the ultrasonic pulse (wideband) to obtain an attenuation-with-frequency curve;
6. Determine the best frequency band within the band width of frequencies in step 5 to obtain a linear fit with respect to frequency;



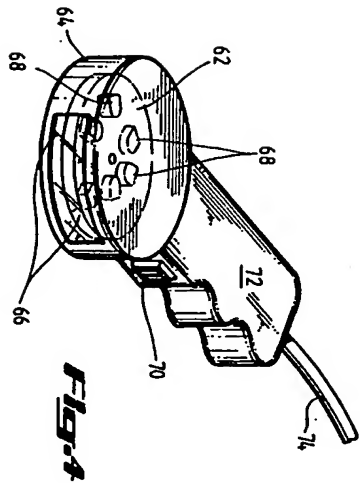


Fig. 4

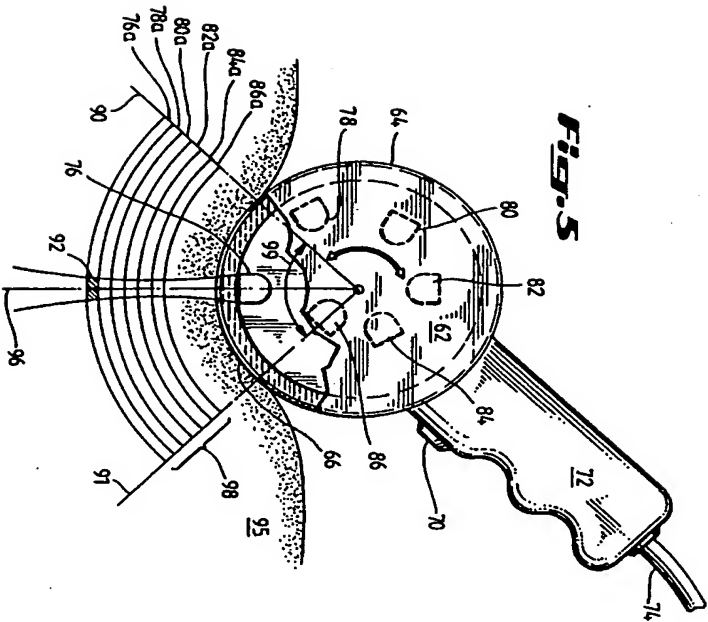


Fig. 5

7

radiation axis 52. As the scanner mechanism turns, transducer 48 is aligned at a separate point along the axis and acquires echoes from region 60. Similarly, transducer 46 is positioned at a unique point along axis 52 and acquires echoes from region 58. As will be appreciated from FIG. 3, the distances 44a, 44b, and 44c between the apertures of transducers 44, 46 and 48 and their respective regions are identical. In this way, the benefits of ABT are achieved, but without the necessity of a bulky water bag. By using matched transducers—i.e., transducers having substantially identical acoustic properties, the scanner of the present invention achieves the same results as a single transducer axially translated along a common axis in a water bag as in FIG. 2. It will also be appreciated that the speed and mechanism of the present invention solves the problem of slow data acquisition which is undesirable in clinical settings.

The present invention may advantageously perform ABT techniques with a scanner as shown in FIG. 4. The scanner comprises a disk 62, rotatably disposed in a sealed housing 64 which contains an acoustic window 66. The acoustic window is sound-permeable and may be constructed from a membrane of a high strength thermoplastic resin, such as a polycarbonate or the like. The housing is filled with an acoustic coupling fluid which is matched to the speed of sound and impedance of the target body. The disk 62 contains a plurality of axially staggered and matched transducer elements 68. As the disk rotates, different transducers will scan the acoustic window 66 at axially different positions along one or more common axes. Because of the staggering of the transducers 68, sequential transducer sweeps will be operable to acquire echo signals from sequentially staggered regions within a target body. As will be apparent from FIG. 4 and FIG. 5, the regions may be staggered both axially and arcuately.

ABT may be achieved by appropriate range gating of the returned echoes such that only echoes returning from regions at a fixed distance from each respective transducer element are received. The range gate may be set, for example, to acquire echo signals corresponding to regions having a width of from about 1 cm to about 3 cm. These echoes may be used to generate an image or may be used to calculate the attenuation coefficient. The diameter of the scanner is usually somewhat larger than twice the depth of the body region of interest targeted for attenuation estimations. In clinical diagnosis, the body contact area may range from about 6 cm X 2 cm to about 9 cm X 2 cm, depending on the number of axially staggered transducers employed. The apparatus may optionally contain a manual ABT switch 70 located in handle 72 of the scanning mechanism. This may allow the operator to obtain an anatomical image before activating the ABT mode. Electrical lead 74 may connect the scanner of FIG. 4 to an ultrasonic display system such as exemplified in FIG. 6.

The apparatus and method of the present invention require a plurality of axially staggered and matched transducers to achieve the advantages of quick, accurate and non-problematic attenuation measurements. Optionally, additional unstaggered transducer elements may be included for conventional imaging only. The invention contemplates transducers which may be piezoelectric, ferroelectric or magnetostrictive in nature. The present invention is not limited by the size, focusing properties or beam width of the transducer elements to be employed.

4,993,416

8

In general, a focused transducer has an ultrasonic beam which in a certain range is constructed or narrower in diameter than the fixed diameter beam generated by a non-focused transducer. The range from the transducer aperture at which a focused beam is constructed is known as the working range of the transducer. Outside that range the focused beam is more divergent than an unfocused beam. In one embodiment of the present invention, a plurality of focused transducers may be used. Sequential transducer sweeps across the acoustic window then have sequentially staggered focal lengths by accepting signals only from the focal (working) range of each transducer element and combining the images so obtained. ABT may be achieved and high resolution imaging in the extended focus may also be simultaneously done. However, the present invention contemplates the use of either focused or unfocused transducers.

The apparatus and method of the present invention are not limited to a particular algorithm for calculating the attenuation characteristics of a target body. The present invention optionally contemplates using a combination of ABT and IDP algorithms to further correct echo spectra obtained during attenuation measurements. For a review of IDP algorithms and techniques, see Carroza, et al., "Diffraction Correction in Pulse Echo Attenuation Measurement," IEEE Ultrasonics Symp. Proc. 84-146, (IEEE Cat. No. 83, CH 194-1, 1983); Croeterman, et al., "A Beam Corrected Estimation of the Frequency Dependent Attenuation of Biological Tissues from Backscattered Ultrasound," Ultrasonic Imaging, Vol. 5, 136-147 (1983); and Issana, et al., "Improvements in the Spectral Difference Method for Measuring Ultrasonic Attenuation," Ultrasonic Imaging, Vol. 5, 331-345 (1983), which are incorporated by reference herein.

For a further review of algorithms used in attenuation characterization, see Lerman et al., "Perspectives on Attenuation Estimation from Pulse-Echo Signals," IEEE Transactions on Sonics and Ultrasonics, Vol. SU-31, No. 4, 352-361 (1984) and Garra, et al., "In Vivo Attenuation Measurement Method and Clinical Relevance," Proc. 6th European Communities Workshop, 87-100 (1988), which are incorporated by reference herein.

Although the apparatus and method of this invention are typically described in relation to clinical diagnosis, this should be understood not to be a limiting factor on the utility of the invention. To the contrary, the present invention has utility in any area in which the attenuation characteristics of a target body may be desired. For example, the present invention may be used in forensic, tissue characterization studies, veterinary medicine, laboratory experiments or measuring the properties of any material which exhibits acoustic attenuation and scattering of ultrasonic energy.

As schematically shown in FIGS. 4 and 5, an ultrasonic scanner having six axially staggered transducer elements 76, 78, 80, 82, 84 and 86 is acoustically coupled to a target body 92. The extended focus sector 98 of the body 92 having boundaries 90 and 91 is diagnosed as the transducers sequentially sweep acoustic window 66. The extended focus sector 98 comprises six range gated strips 76a, 78a, 80a, 82a, 84a and 86a which correspond to the six axially staggered transducer elements. The sector angle 99 may be determined by the number of transducer elements. For example, six transducer elements allow a $2\pi/6$ or $\pi/3$ sector angle 99. The range

In (D3) $d = R - W$ is the portion of R for which α is non-zero, and W is the portion for which α is zero. Assuming that there are two scattering ensembles at ranges R_1 and R_2 , respectively, having the same average value for $\langle \alpha^2 \rangle$ and both within the attenuating target body (see FIG. 1, regions 22 and 24), then the ratio of the received ultrasound echo from both ranges is:

$$\frac{P_R(R_1)}{P_R(R_2)} = \exp \left[\frac{\ln(d_1 - d_2)}{(R_1/R_2)^2} \right] \quad (D3)$$

The variables d_1 and d_2 may be expressed as $R_1 - W$ and $R_2 - W$, respectively. The constant speed of sound in the water path mechanism is assumed to be the same as that of the target body (tissue). The wavelength of the ultrasound pulse is also assumed constant. The numerator of (D3) contains the desired attenuation information, whereas the denominator is a beam-spreading loss which causes artifacts in acquired echoes and results in bias errors in estimating the attenuation characteristics of the target body.

A reduction in the effect of beam-spreading loss can be achieved by performing attenuation measurements such that the acquisition of echo spectra is done in two steps (see FIG. 2): (1) echoes are acquired from a given range $R = R_1 = R_2$ first, and then (2) the transducer is translated along its radiation axis in a water path by a known amount $(d_1 - d_2)$ and echoes are again acquired at the same range R from the transducer, but which emanate from a new depth in the target body. The preservation of the range reduces the beam-spreading loss. Thus, if R_1 and R_2 are equal, but d_1 and d_2 are not, then (D3) becomes:

$$\frac{P_R(d_1)}{P_R(d_2)} = \exp[\alpha(d_1 - d_2)] \quad (D4)$$

The variable P_R is proportional to the square of the received echo converted to a voltage V_r . Solving (D4) for α in units of decibels ("dB") per centimeter ("cm"), yields:

$$\alpha(\text{dB/cm}) = 0.57 \frac{\log_{10}[P_R(d_1) - \log_{10}[P_R(d_2)]]}{d_1 - d_2} \quad (D5)$$

In (D5) the expression for α is independent of $\langle \alpha^2 \rangle$, as long as it is assumed to remain constant. Also, (D5) is only valid for a single discrete frequency. This equation can be generalized for a wide band spectrum as:

$$\alpha(f)(\text{dB/cm/MHz}) = 0.57 \frac{\log_{10}[P_R(f, d_1) - \log_{10}[P_R(f, d_2)]]}{d_1 - d_2} \quad (D6)$$

The value of $\alpha(f)$ is the frequency slope of the attenuation coefficient, and $V_r(f, d_1)$ and $V_r(f, d_2)$ are the average spectra of the echoes at depths d_1 and d_2 , respectively. Equation (D6) essentially describes the simplest form of the log-spectral difference method, but with the added important feature that bias errors due to beam-spreading loss are reduced by ABT.

The log-spectral difference method for measuring attenuation with a fixed transducer is exemplified in FIG. 1. The transducer 10 is shown acoustically coupled to an organic body 12. The ultrasonic beam 20 is shown propagating into the body 12 along its radiation axis 18. The ultrasonic echo sequence propagates along the radiation axis 18 opposite the ultrasonic beam

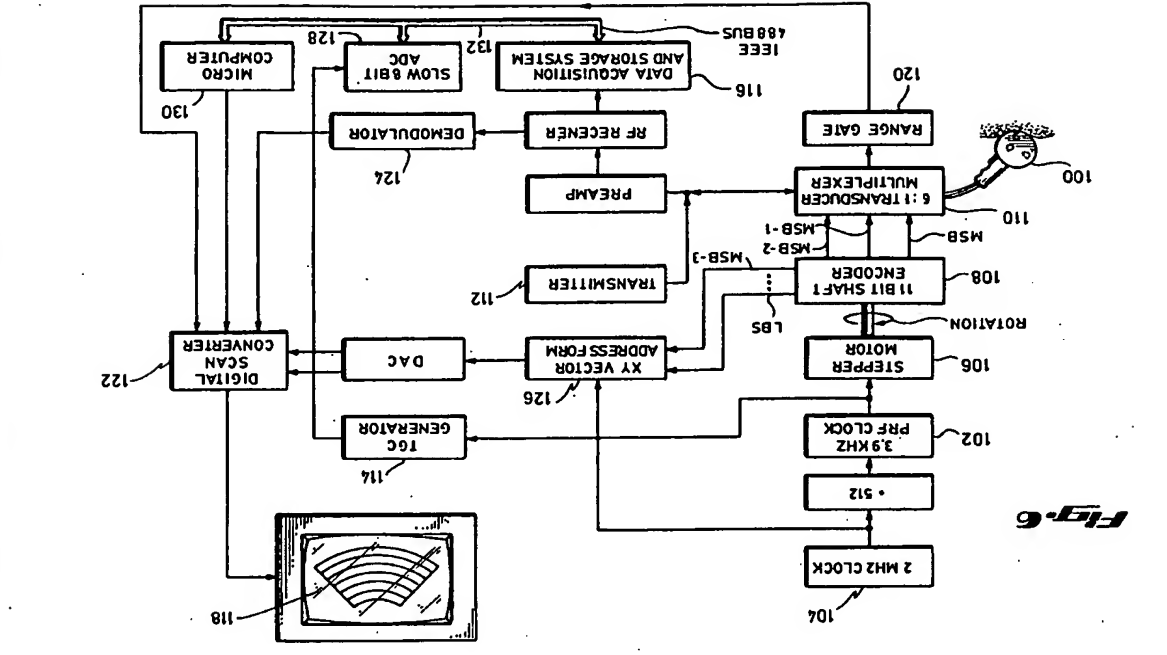


Fig. 6

FIG. 2 exemplifies the use of ABT to reduce the bias errors in the attenuation estimation discussed above. Transducer 30 is shown disposed in water path 35 which is acoustically coupled to body 34. Echoes are acquired from region 38 in response to acoustic beam 36 using range gating techniques as set forth above. The transducer 30 is then translated along the radiation axis 40 to position 30a wherein echoes from region 42 are acquired. The distance between aperture 32 and region 38 is identical to the distance between the aperture at 32a and region 42. By keeping the distance between each transducer aperture and its respective region of interest constant during echo acquisition, the bias errors in the derived attenuation coefficient may be reduced.

The present invention utilizes ABT techniques to reduce bias errors in attenuation estimations without the need for a bulky water bag. According to the present invention, ABT may be conveniently performed by utilizing a plurality of matched transducers mounted on a scanning mechanism in an axial stagger pattern. As a result of the pattern, the mechanism will sequentially place each respective transducer across an acoustic window at axially different positions along one or more common axes.

Conveniently, the present invention may employ a rotating scanning head which carries a plurality of transducers. As illustrated in FIG. 3, transducers 44, 46 and 48 are mounted on a rotor 50 and face radially outward in a spirally staggered pattern. As the rotor 50 turns, the transducers are sequentially positioned at different points along the axis 52 and thus become axially staggered. As each transducer sweeps past the axis 52, an ultrasonic pulse 54 is generated and echo spectra acquired for temporal windows corresponding to regions 56, 58 and 60. For example, transducer 44 is used to acquire echoes from region 56 along the ultrasonic

SYSTEM FOR ULTRASONIC PAN FOCAL IMAGING AND AXIAL BEAM TRANSLATION

BACKGROUND OF THE INVENTION

1. Field of the Invention

This invention relates generally to methods and apparatus for performing ultrasonic diagnosis of a target body and more particularly to methods and apparatus for concomitantly acquiring an ultrasonic image and measuring the attenuation characteristics of a target body.

2. Description of Related Art

Traditional ultrasonic diagnosis is performed by transmitting ultrasonic energy into a target body and generating an image from the resulting echo signals in order to survey anatomical structures. A transducer is used to both transmit the ultrasonic energy and to receive the echo signals. During transmission, the transducer converts electrical energy into mechanical vibrations. Acquired echo signals produce mechanical oscillations in the transducer which are converted to electrical signals for amplification and recognition.

A human or animal body represents a non-homogeneous medium for the propagation of ultrasound energy. Images may be generated from the echo/backscatter signals which are produced as ultrasonic energy propagates through acoustic impedance interfaces and lower level scatter sites within the target body.

Acoustic impedance changes at boundaries of varying density and/or sound speed within a target body. A portion of the incident ultrasonic beam is reflected at these boundaries. Inhomogeneities within the target medium from lower-level scatter sites which result in additional echo signals. Tissue characterization may be measured from acoustic attenuation and acoustic impedance changes at the boundaries and the scatter sites. A knowledge of the speed of sound in tissue permits the determination of the depth and location of both the interfaces and the echo sites from the measurement of echo travel time. An image may be generated from this information by modulating the intensity of pixels on a display in proportion to the intensity of echoes from corresponding points in the target.

In recent years, much effort has been expended to obtain clinically useful data from the several physical processes involved in echo production. In particular, techniques for measuring the attenuation of ultrasonic energy as it propagates through a soft tissue have been pursued. As ultrasonic energy propagates through tissue, some of the energy is absorbed and some is scattered out of the acoustic pathway. These two mechanisms result in a net loss of signal power—i.e., acoustic attenuation. Acoustic attenuation has a near linear frequency dependence and is generally characterized as signal power loss in decibels per centimeter of propagation per MHz. When attenuation is plotted as a function of frequency, a near linear relationship is defined. This function—the attenuation coefficient—varies with the acoustic characteristics of particular tissues. In soft tissues it has been shown that there is some correlation between attenuation characteristics and tissue pathology. For example, a healthy liver will have a different attenuation coefficient than a cirrhotic liver. Thus, a technique for accurate measurement of acoustic attenuation characteristics would be clinically valuable.

Several prior art techniques have been developed to measure the attenuation characteristics of soft tissue.

One prior art technique for measuring ultrasound attenuation requires that the target body be placed between separate transmitting and receiving transducers. This technique, however, is impractical in clinical settings, since transmission through most sections of a target body is not possible.

A second prior art technique known as the "substitution method" utilizes a known reflector to return echoes to a common transmitting/receiving transducer. A tissue specimen is placed between the transducer and the reflector, and the resulting decrease in echo signal power is used to determine the attenuation characteristics of the tissue. This technique, however, also has clinical limitations, since known reflectors cannot be inserted into human target bodies.

Both of the above prior art techniques are further limited by the measurement of attenuation based upon the entire path of the propagating energy. As such, they are not entirely suitable for measuring attenuation of limited regions of interest within a target body.

Knowledge of the ultrasound attenuation characteristics within limited regions of a human or other animal target body has specific value for clinical diagnostic purposes. As discussed above, for example, diseased livers have different attenuation characteristics from healthy ones. A technique known as the "spectral difference" method has been proposed, whereby echo signals from varying depths in the target are acquired and converted to spectral signals using known Fourier transform algorithms. See Roman, Kase, "Estimating Acoustic Attenuation from Reflected Ultrasonic Signals: Comparison of Spectral Shift and Spectral Difference Approaches", IEEE Transactions on Acoustics, Speech and Signal Processing, ASSP-32, 1-6, (1984). A knowledge of the speed of sound in the target allows the ultrasonic echo sequence to be broken up into temporal spectral windows which correspond to varying depths in the target. The log-spectral differences between windows are computed, and the attenuation coefficient is derived. However, attenuation estimations using this technique tend to suffer from bias errors. These errors are attributable to a variety of phenomena, including the inherent differences in pulse-echo impulse response of a transducer at various distances from the transducer aperture.

One method for eliminating the effects of these beam diffraction errors has used Inverse Diffraction Filtering ("IDF") techniques to develop a beam correction factor. IDF techniques utilize plane reflectors or tissue mimicking phantoms to measure the differences in pulse-echo impulse response of a transducer as a function of range to derive a beam correction function. However, these beam correction functions are not entirely satisfactory in clinical settings since pulse-echo beam characteristics may vary in different tissues, particularly in unknown tissues. See Robinson, et al., "Beam Pattern Measurement", Correction for Ultrasonic Attenuation (Diffraction) Ultrasonic Imaging, Vol. 6 No. 3, 293-303 (1984). Thus, the IDF correction factor to be applied to echo signals varies according to the type of (generally unknown) tissue being examined.

A second method for elimination of diffraction errors known as Axial Beam Translation ("ABT") has been successful in rendering unbiased estimations of attenuation in unknown targets. See Ogbih and Melsa, "Elimination of Diffraction Error in Acoustic Attenuation Estimation Via Axial Beam Translation", Ultrasonic

Imaging 10, 139-152 (1988) which is incorporated by reference herein. However, initial ABT techniques have tended to be problematic in clinical settings due to the requirement for axial translation of the transducer in a bulky water bag. Also, these initial ABT techniques require several minutes to collect sufficient ultrasonic echo data for accurate attenuation estimations. This time requirement is not very desirable for current medical diagnosis purposes. Thus, until the present invention, ABT techniques have not been adaptable to current ultrasonic imaging systems.

Several forms of ultrasonic scanning mechanisms have been suggested for use in performing ultrasonic diagnosis of human and animal organs. One principal form employs a rotating scanning head which carries a plurality of transducers. As the head rotates, the transducers sequentially pass by a body organ at which time they transmit signals into the organ and receive reflected echoes from the organ.

A second principal form of ultrasonic scanning mechanism employs an oscillating scanning head or "wobbler" which normally has a single transducer. As the head oscillates, the transducer oscillates through a scanned angle while transmitting and receiving ultrasonic signals.

In both the rotating and oscillating scanning mechanisms, the scanning head may be mounted in a housing filled with an acoustic coupling liquid. In some instances, the motor driving the head may be mounted directly in the same liquid-filled housing; in other instances, it may be mounted in a dry region outside the housing and coupled to the head through a suitable seal.

SUMMARY OF THE INVENTION

The method and apparatus of the present invention address the problems inherent in the prior art, including the bulky water bag and the slow data acquisition of the known ABT methods. The present invention provides a novel method and apparatus which allows concomitant imaging and rapid ABT measurements. The present invention also enables ABT to be adapted to current ultrasonic imaging systems.

The present invention comprises a method and apparatus for concomitant ultrasonic pan focal imaging and axial beam translation. The present invention employs an ultrasonic scanner which contains a plurality of matched transducer elements. These elements are staggered on a mechanism which sequentially places each transducer opposite an acoustic window at axially spaced positions along a common ultrasonic radiation axis. Further, the mechanism may scan across the window so that the transducers may repeat this axial other along a plurality of such radiation axes which radiate through the same window. Thus, the invention comprises a system for scanning a region within a tissue or similar target body by tracking or stepping laterally across the target with an axial array of transducers which transmit and receive sonic signals to and from the target along a plurality of different radiation axes or sonic travel paths. The transducers are positioned on a movable mounting means or mechanism such that the transducers are axially spaced from one another along each said axis or sonic travel path. Normally, the transducers are not axially arrayed on the mechanism itself but instead are sequentially positioned or staggered along a common radiation axis or axis by movements of the mechanism. Hence, the transducers are considered for the purposes of the invention to be axially staggered.

Because of the axial staggering of the elements, sequential transducer scans may acquire echo data emanating from successively deeper or shallower regions in the target body corresponding to the stagger pattern. Each region being scanned is at a constant range from its respective transducer element. In this way, ABT is achieved and an extended or pan focal image may also be concomitantly acquired by appropriate range gating of the returned echoes for each respective transducer. The apparatus and method of the present invention is a safe and non-invasive mechanism for the diagnosis of organic tissue. It allows tissue pathology to be detected without the need for biopsy and other surgical techniques.

Other objects and advantages and a more complete understanding of the invention may be obtained by referring to the following detailed description when taken in conjunction with the accompanying drawings.

BRIEF DESCRIPTION OF THE DRAWINGS

FIG. 1 is a schematic view useful for explaining variations in impulse response of a transducer to echoes originating at different points along its ultrasonic radiation axis.

FIG. 2 is a schematic view useful for explaining the elimination of diffraction error in acoustic attenuation measurement using axial beam translation.

FIG. 3 is a schematic view useful for explaining an axial stagger pattern of matched transducers according to of the present invention.

FIG. 4 is a perspective interior view of an ultrasonic scanner according to one apparatus embodiment of the present invention.

FIG. 5 is a schematic interior view of the ultrasonic scanner of FIG. 4 shown acoustically coupled to a target body.

FIG. 6 is a block diagram of an ultrasonic diagnosis system according to one embodiment of the present invention.

DETAILED DESCRIPTION

The Axial Beam Translation ("ABT") method relies on the acquisition of echoes from varying depths in the target body, while maintaining a constant range from the transducer aperture. The ratio between the received (echo) and transmitted (pulsed) of ultrasonic power for backscatter from an ensemble of scatterers in the far field of an ultrasonic transducer can be expressed as:

$$\frac{P_{R0}}{P_T} = \frac{I_0 \langle \sigma \rangle \lambda^2 \sin^2 \theta}{P_T \lambda^2} \quad (1)$$

The variable R is the distance from the transducer to the scatterers, λ is the wavelength, assuming a fixed frequency, T is the efficiency of the transducer, A is the effective aperture of the transducer, α is the attenuation coefficient of the target body at frequency $f = c/\lambda$ (where c is the speed of sound propagation in the target body), and $\langle \sigma \rangle$ is the average backscatter cross section. If the medium between the transducers and the scatterers is composed of attenuating (lossy) and non-attenuating (lossless) parts, then (1) can be rewritten as:

$$\frac{P_{R0}}{P_T} = \frac{I_0 \langle \sigma \rangle \lambda^2 \sin^2 \theta}{P_T \lambda^2} e^{-2\alpha R} \quad (2)$$

UNITED STATES PATENT AND TRADEMARK OFFICE
CERTIFICATE OF CORRECTION

PATENT NO. : 4,993,416

DATED : Feb. 19, 1991

INVENTOR(S) : Jonathan Ophir

It is certified that error appears in the above-identified patent and that said Letters Patent
is hereby corrected as shown below:

Column 11, line 13, before "tissue" insert "--ultrasonic--."

Signed and Sealed this

Fifteenth Day of December, 1992

Attest:

DOUGLAS B. COMER

Acting Commissioner of Patents and Trademarks

Attesting Officer

THIS PAGE BLANK (USPTO)